Middle East respiratory syndrome coronavirus and bat coronavirus HKU9 both can utilize GRP78 for attachment onto host cells

Received for publication, January 22, 2018, and in revised form, May 26, 2018 Published, Papers in Press, June 10, 2018, DOI 10.1074/jbc.RA118.001897

Hin Chu[a,b1], Che-Man Chan[a,b1], Xi Zhang[b1], Yixin Wang[b], Shuofeng Yuan[b], Jie Zhou[a,b], Rex Kwok-Him Au-Yeung[c], Kong-Hung Sze[a,b], Dong Yang[b], Huiping Shuai[b], Yuxin Hou[b], Cun Li[b], Xiaoyu Zhao[b], Vincent Kwok-Man Poon[b], Sze Pui Leung[b], Man-Lung Yeung[a,b,d,e], Jinghua Yan[f], Guangwen Lu[g], Dong-Yan Jin[h], George Fu Gao[f,i], Jasper Fuk-Woo Chan[a,b,d,e2,3], and Kwok-Yung Yuen[a,b,d,e,j2,4]

From the [a]State Key Laboratory of Emerging Infectious Diseases, Departments of [b]Microbiology and [c]Pathology, [d]Research Centre of Infection and Immunology, [e]Carol Yu Centre for Infection, [h]School of Biomedical Sciences, and [j]Collaborative Innovation Center for Diagnosis and Treatment of Infectious Diseases, Li Ka Shing Faculty of Medicine, University of Hong Kong, Pokfulam, Hong Kong Special Administrative Region, the [f]CAS Key Laboratory of Pathogenic Microbiology and Immunology, Institute of Microbiology, Chinese Academy of Sciences, Beijing 100101, the [g]West China Hospital Emergency Department, State Key Laboratory of Biotherapy, West China Hospital, Sichuan University, and Collaborative Innovation Center of Biotherapy, Chengdu, Sichuan 610041, and the [i]National Institute for Viral Disease Control and Prevention, Chinese Center for Disease Control and Prevention (China CDC), Beijing 102206, China

Edited by Charles E. Samuel

Coronavirus tropism is predominantly determined by the interaction between coronavirus spikes and the host receptors. In this regard, coronaviruses have evolved a complicated receptor-recognition system through their spike proteins. Spikes from highly related coronaviruses can recognize distinct receptors, whereas spikes of distant coronaviruses can employ the same cell-surface molecule for entry. Moreover, coronavirus spikes can recognize a broad range of cell-surface molecules in addition to the receptors and thereby can augment coronavirus attachment or entry. The receptor of Middle East respiratory syndrome coronavirus (MERS-CoV) is dipeptidyl peptidase 4 (DPP4). In this study, we identified membrane-associated 78-kDa glucose-regulated protein (GRP78) as an additional binding target of the MERS-CoV spike. Further analyses indicated that GRP78 could not independently render nonpermissive cells susceptible to MERS-CoV infection but could facilitate MERS-CoV entry into permissive cells by augmenting virus attachment. More importantly, by exploring potential interactions between GRP78 and spikes of other coronaviruses, we discovered that the highly conserved human GRP78 could interact with the spike protein of bat coronavirus HKU9 (bCoV-HKU9) and facilitate its attachment to the host cell surface. Taken together, our study has identified GRP78 as a host factor that can interact with the spike proteins of two *Betacoronaviruses*, the lineage C MERS-CoV and the lineage D bCoV-HKU9. The capacity of GRP78 to facilitate surface attachment of both a human coronavirus and a phylogenetically related bat coronavirus exemplifies the need for continuous surveillance of the evolution of animal coronaviruses to monitor their potential for human adaptations.

This work was supported in part by the donations of Michael Seak-Kan Tong, Hui Ming, Hui Hoy and Chow Sin Lan Charity Fund Limited, Chan Yin Chuen Memorial Charitable Foundation, and the Providence Foundation Limited in memory of the late Dr. Lui Hac Minh; Hong Kong Health and Medical Research Fund Grants 14131392, 15140762, and 16150572; National Natural Science Foundation of China/Research Grants Council (NSFC/RGC) Joint Research Scheme Grants N_HKU728/14 and 81461168030; Theme-Based Research Scheme Grant T11/707/15 of the Research Grants Council, Hong Kong Special Administrative Region, and by funding from the Ministry of Education of China for the Collaborative Innovation Center for Diagnosis and Treatment of Infectious Diseases. The authors declare that they have no conflicts of interest with the contents of this article.

This article contains Figs. S1–S4.

[1] These authors contributed equally to this work.

[2] Co-senior authors.

[3] To whom correspondence may be addressed: State Key Laboratory of Emerging Infectious Diseases, Carol Yu Centre for Infection, Dept. of Microbiology, University of Hong Kong, Queen Mary Hospital, 102 Pokfulam Rd., Pokfulam, Hong Kong Special Administrative Region, China. Tel.: 852-22554897; Fax: 852-28551241; E-mail: jfwchan@hku.hk.

[4] To whom correspondence may be addressed: State Key Laboratory of Emerging Infectious Diseases, Carol Yu Centre for Infection, Dept. of Microbiology, University of Hong Kong, Queen Mary Hospital, 102 Pokfulam Rd., Pokfulam, Hong Kong Special Administrative Region, China. Tel.: 852-22554897; Fax: 852-28551241; E-mail: kyyuen@hku.hk.

Coronaviruses are known to infect a broad spectrum of species, ranging from birds to mammals, including humans (1–3). They are enveloped RNA viruses with large genome sizes of ~28–32 kb. Currently, coronaviruses are classified into four genera: *Alphacoronavirus, Betacoronavirus, Gammacoronavirus,* and *Deltacoronavirus* (4). Among them, six coronaviruses from the *Alphacoronavirus* genera and the *Betacoronavirus* genera are known to cause human infections with diverse outcomes. On the one hand, human coronavirus 229E (HCoV-229E),[5] human coronavirus NL63 (HCoV-NL63), human coro-

[5] The abbreviations used are: HCoV, human coronavirus; MERS-CoV, Middle East respiratory syndrome coronavirus; SARS-CoV, severe acute respiratory syndrome coronavirus; DC-SIGN, dendritic cell-specific intercellular adhesion molecule-3-grabbing nonintegrin; RBD, receptor-binding domain; qPCR, quantitative PCR; MDM, monocyte-derived macrophage; MFI, mean fluorescent intensity; HFL, human embryonic lung fibroblast; ER, endoplasmic reticulum; DMEM, in Dulbecco's modified Eagle's medium; FBS, fetal bovine serum; PBMC, peripheral blood mononuclear cell; LP, lentiviral particle; m.o.i., multiplicity of infection; RLU, relative light unit; BAP, bacterial

navirus OC43 (HCoV-OC43), and human coronavirus HKU1 (HCoV-HKU1) predominantly cause mild and self-limiting upper respiratory tract infections (5, 6). In stark contrast, severe acute respiratory syndrome coronavirus (SARS-CoV) that caused the severe acute respiratory syndrome epidemic between 2002 and 2003 was highly pathogenic, which infected more than 8000 people with a fatality rate of ~10% (7, 8). Ten years later, another highly pathogenic human coronavirus, Middle East respiratory syndrome coronavirus (MERS-CoV), emerged in the Middle East in 2012 (9). MERS-CoV caused severe lower respiratory tract infections with an exceptionally high fatality rate of ~35%. Most importantly, despite global efforts trying to control the virus' dissemination, MERS-CoV still spread to over 27 countries and has been causing continuous infections in the Middle East since 2012 (10).

The interaction between the spike protein and its receptor is the main determinant of host tropism for coronaviruses (11). Among the six human coronaviruses, the *Alphacoronavirus* HCoV-229E spike binds aminopeptidase N (12), whereas the lineage C *Betacoronavirus* the MERS-CoV spike recognizes dipeptidyl peptidase 4 (DPP4) (13). Intriguingly, the *Alphacoronavirus* HCoV-NL63 and the lineage B *Betacoronavirus* SARS-CoV both utilize angiotensin-converting enzyme 2 (ACE2) for cell entry (14, 15). However, the protein receptors for the lineage A *Betacoronavirus* HCoV-OC43 and HCoV-HKU1 are currently unknown. In addition to their designated receptors, coronavirus spikes are known to recognize a broad array of cell-surface molecules, which serve to facilitate the attachment or entry of the viruses. For example, HCoV-NL63 and mouse hepatitis virus both employ heparan sulfate proteoglycans to enhance attachment (16, 17). Similarly, transmissible gastroenteritis coronavirus, bovine coronavirus, HCoV-OC43, and HCoV-HKU1 bind to *O*-acetylated sialic acid as key attachment molecules (18–21). Interestingly, in addition to utilizing *O*-acetylated sialic acid as a critical binding determinant (21), HCoV-HKU1 spike also recognizes major histocompatibility complex class I C as another attachment molecule (22). In the case of SARS-CoV, dendritic cell–specific intercellular adhesion molecule-3– grabbing nonintegrin (DC-SIGN) and DC-SIGN–related both augment virus entry (23, 24). For MERS-CoV, we previously reported carcinoembryonic antigen-related cell adhesion molecule 5 (CEACAM5) as an attachment factor that could modulate MERS-CoV entry in permissive cells (25). More recently, tetraspanin CD9 was identified as a host cell- -surface factor that facilitated MERS-CoV entry by scaffolding host cell receptors and proteases (26).

Knowledge of the interaction between coronavirus spikes and cell-surface host factors contributes to the understanding of coronavirus biology on many aspects, including tropism, pathogenicity, as well as potential intervention strategies. To this end, we aimed to investigate whether additional cell-surface molecules were involved in the attachment or entry of MERS-CoV. In this study, we reported that the MERS-CoV spike could recognize a 78-kDa glucose–regulated protein (GRP78). Although traditionally regarded as an ER protein with chaperone activity, recent discoveries suggest that GRP78 is also localized to the cell surface, where they carry out physiological functions that regulate signaling and cellular homeostasis (27). Subsequent experiments demonstrated that GRP78 did not render nonpermissive cells susceptible to MERS-CoV infection but played a positive role in augmenting MERS-CoV entry in permissive cells, suggesting that GRP78 is an attachment factor of MERS-CoV that can modulate MERS-CoV entry in the presence of the host cell receptor DPP4. Importantly, our data further indicated that the spike protein of a lineage D *Betacoronavirus*, bat coronavirus HKU9 (bCoV-HKU9), also recognized GRP78, which played a key role in the attachment of HKU9–S-pseudovirus to the bat *Rousettus leschenaulti* kidney (RLK) cells. Our findings highlight the importance of the possible evolution of different animal and human coronaviruses to become capable of using not just the same host receptors but also the same attachment factors, which may facilitate animal coronaviruses to jump the interspecies barrier into human.

Results

GRP78 interacts with MERS-CoV spike

We previously identified human carcinoembryonic antigen-related cell adhesion molecule 5 (CEACAM5) as an attachment factor for MERS-CoV (25). In this study, we asked whether additional membrane proteins could interact with the MERS-CoV spike and facilitate the entry or attachment of MERS-CoV. To this end, we transfected human bronchus epithelial cells, BEAS2B, with the MERS-CoV spike and evaluated the membrane proteins that might bind the MERS-CoV spike in the transfected cells. In brief, membrane proteins from pcDNA–MERS-CoV–S1–V5-transfected BEAS2B cells were extracted and sedimented (Fig. 1). To evaluate the extraction efficiency, the cell extracts were probed for markers of different cellular fractions, including that of the plasma membrane (epidermal growth factor receptor (EGFR) and pan-cadherin), endoplasmic reticulum (ER) (calreticulin), Golgi (giantin), and nucleus (lamin A). Western blotting analyses revealed that our membrane extracts were enriched with the plasma membrane markers, EGFR and pan-cadherin. In contrast, only a trace amount of the ER marker was observed, whereas the signal for Golgi and nucleus was not detected (Fig. 1*D* and Fig. S1).

To identify potential proteins that could interact with the MERS-CoV spike, the membrane extracts were immunoprecipitated with a V5 mAb and protein A/G-Sepharose. The precipitated beads were then washed, and protein complexes were eluted with 0.1 M glycine. Co-immunoprecipitated proteins were revealed in SDS-PAGE after silver staining (Fig. 1*A*, *lane 1*). The eluted beads were resuspended in sample loading buffer, boiled, and assessed for elution efficiency (Fig. 1*A*, *lane 2*). As a control, the same set of membrane extracts was immunoprecipitated with isotype antibody and protein A/G-Sepharose (Fig. 1*A*, *lane 3*). In parallel, the expression of the MERS-CoV spike in the immunoprecipitated complexes was validated

alkaline phosphatase; EGFR, epidermal growth factor receptor; co-IP, co-immunoprecipitation; DAPI, 4,6-diamidino-2-phenylindole; VSV-G, vesicular stomatitis virus glycoprotein; eGFP, enhanced GFP.

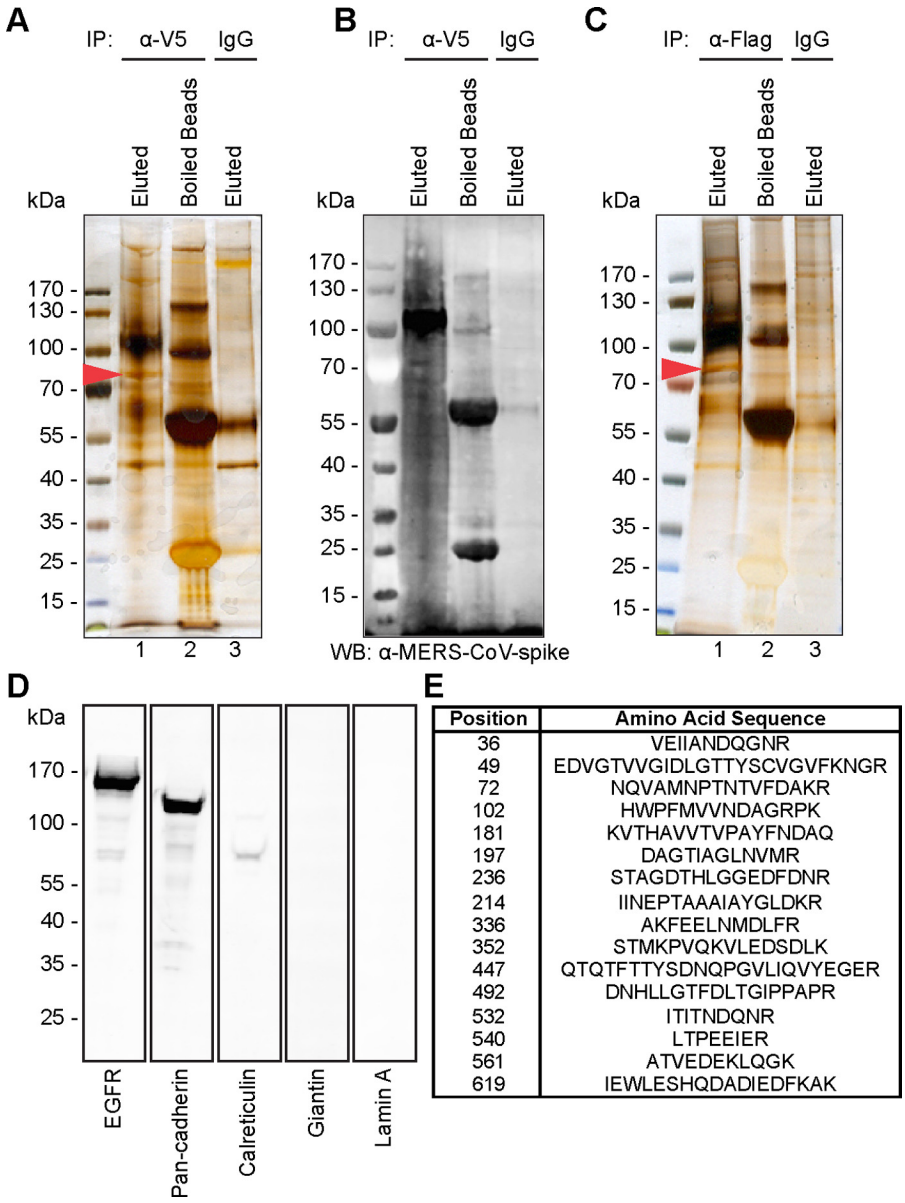

Position	Amino Acid Sequence
36	VEIIANDQGNR
49	EDVGTVVGIDLGTTYSCVGVFKNGR
72	NQVAMNPTNTVFDAKR
102	HWPFMVVNDAGRPK
181	KVTHAVVTVPAYFNDAQ
197	DAGTIAGLNVMR
236	STAGDTHLGGEDFDNR
214	IINEPTAAAIAYGLDKR
336	AKFEELNMDLFR
352	STMKPVQKVLEDSDLK
447	QTQTFTTYSDNQPGVLIQVYEGER
492	DNHLLGTFDLTGIPPAPR
532	ITITNDQNR
540	LTPEEIER
561	ATVEDEKLQGK
619	IEWLESHQDADIEDFKAK

Figure 1. Identification of GRP78 as a target membrane protein of the MERS-CoV spike. *A,* silver staining of membrane proteins of BEAS2B cells transfected with pcDNA–MERS-CoV–S1–V5. Membrane extracts were immunoprecipitated (*IP*) with V5 antibody and Sepharose A/G beads, followed by washing and eluting with glycine (*lane 1*). Sepharose beads were boiled in sample buffer after glycine elution (*lane 2*). Membrane extracts were immunoprecipitated with mouse isotype control and Sepharose A/G beads (*lane 3*). *B,* expression of MERS-CoV–S1-V5 was detected by Western blotting (*WB*) with an anti-ERS-CoV spike antibody. *C,* silver staining of membrane proteins of BEAS2B cells. The membrane extracts were immunoprecipitated with purified recombinant MERS-CoV–S1–FLAG protein using anti-FLAG M2 antibody and Sepharose A/G beads, followed by washing and eluting with 3× FLAG peptides (*lane 1*). Sepharose beads were boiled in sample buffer after 3× FLAG peptide elution (*lane 2*). Membrane extracts were immunoprecipitated with mouse isotype control and Sepharose A/G beads (*lane 3*). *D,* 5 μg of sedimented membrane extracts were run on SDS-PAGE and subjected to Western blots using antibodies against the plasma membrane marker (EGFR and pan-cadherin), endoplasmic reticulum marker (calreticulin), Golgi marker (giantin), and nucleus marker (lamin A). *E,* gel fragment indicated by the *red arrowhead* in *A* and *C* was excised for LC-MS/MS analysis. MS/MS data were searched against all mammalian protein databases in NCBI and Swiss-Prot. The protein was identified as GRP78 with significant hits over different domains of the sequence.

with Western blotting using a mouse immune serum against the MERS-CoV spike (Fig. 1*B*). Specific protein bands that were pulled down by the V5 antibody but not the isotype control were excised and sent for MS analysis. The MS/MS result revealed one of the dominant bands (Fig. 1*A*, *lane 1, arrowhead*) to be 78-kDa glucose-regulated protein (GRP78), also known as heat shock 70-kDa protein 5 (HSPA5) or binding immunoglobulin protein (BiP) (Fig. 1*E*).

To further verify the interaction between the MERS-CoV spike and GRP78, we attempted to immunoprecipitate GRP78 with purified the MERS-CoV spike proteins. To this end, recombinant MERS-CoV–S1–FLAG proteins were expressed, purified, and immunoprecipitated against the membrane protein extracts from BEAS2B cells. Notably, silver staining of the SDS-PAGE and the subsequent MS confirmed the presence of GRP78 in the precipitated MERS-CoV–S1–FLAG complex (Fig. 1*C*, *lane 1, arrowhead*) but not in the control (Fig. 1*C*, *lane 3*). Taken together, our membrane pulldown assay identified GRP78 as a potential membrane protein specifically bound by the MERS-CoV spike.

GRP78 is a specific binding target of MERS-CoV spike

Next, to examine the direct interaction between GRP78 and the MERS-CoV spike, we performed a series of co-immunoprecipitation (co-IP) assays in both overexpression and endogenous settings. First, BHK21 cells were transfected with GRP78–V5 or the pcDNA–V5 control vector. The cell lysates of the transfected cells were then immunoprecipitated with either MERS-CoV–S1–FLAG or *Escherichia coli* bacterial alkaline phosphatase–FLAG (BAP–FLAG) pre-adsorbed on anti-FLAG M2-agarose beads. The precipitated protein complexes were then detected by Western blotting with the anti-FLAG or the anti-V5 antibody. As illustrated in Fig. 2*A*, GRP78 specifically immunoprecipitated with MERS-CoV–S1 (*lower panel, lane 1*) but not the control bait protein, BAP (*lower panel, lane 2*). Additionally, GRP78 was not precipitated in cells transfected with the empty vector (Fig. 2*A*, *lower panel, lane 3*). To confirm the interaction between GRP78 and MERS-CoV–S1, we performed reciprocal co-IP using GRP78 as the bait protein (Fig. 2*B*). In this setting, cell lysates of GRP78–V5 or empty vector transfected BHK21 cells were immunoprecipitated with anti-V5 pre-adsorbed protein A/G-Sepharose and incubated with purified MERS-CoV–S1–FLAG or BAP–FLAG. Our result demonstrated that MERS-CoV–S1–FLAG but not BAP–FLAG was efficiently immunoprecipitated by GRP78–V5 (Fig. 2*B*, *upper panel, lanes 1* and *2*). As a negative control, the expression of pcDNA–V5 empty vector failed to immunoprecipitate with MERS-CoV–S1–FLAG (Fig. 2*B*, *upper panel, lane 3*). In parallel, MERS-CoV–S1–FLAG did not co-IP with the abundantly expressed cell-surface protein EGFR, suggesting the interaction between MERS-CoV–S1–FLAG and GRP78 was specific (Fig. S2, *A* and *B*). Next, we evaluated whether the interaction between the MERS-CoV spike and GRP78 could occur at the cell surface. To this end, we obtained the membrane fraction of Huh7 cells that was predominantly enriched with the plasma membrane contents of the cells. We then added MERS-CoV–S1–FLAG protein to the membrane extracts and performed co-IP between the MERS-CoV spike and GRP78. Our data showed that the MERS-CoV spike and the endogenous GRP78 in the membrane extract could efficiently interact with each other (Fig. 2, *C* and *D*).

To further verify the physical interaction between GRP78 and the MERS-CoV spike in a physiological relevant scenario, we performed endogenous co-IP experiments in MERS-CoV–infected Huh7 and BEAS2B cells (Fig. 2*E*). In line with our earlier findings, GRP78 efficiently immunoprecipitated the MERS-CoV spike from cell lysates of the infected samples. In contrast, the MERS-CoV spike was not detected from the mock-infected samples or from infected samples immunoprecipitated with a control isotype antibody. The reciprocal co-IP performed using the MERS-CoV spike as the bait similarly immunoprecipitated endogenous GRP78 from the infected samples but not from mock-infected samples or from infected samples immunoprecipitated with the control isotype antibody (Fig. 2*E*). Collectively, our co-IP data established GRP78 as a specific binding target of the MERS-CoV spike.

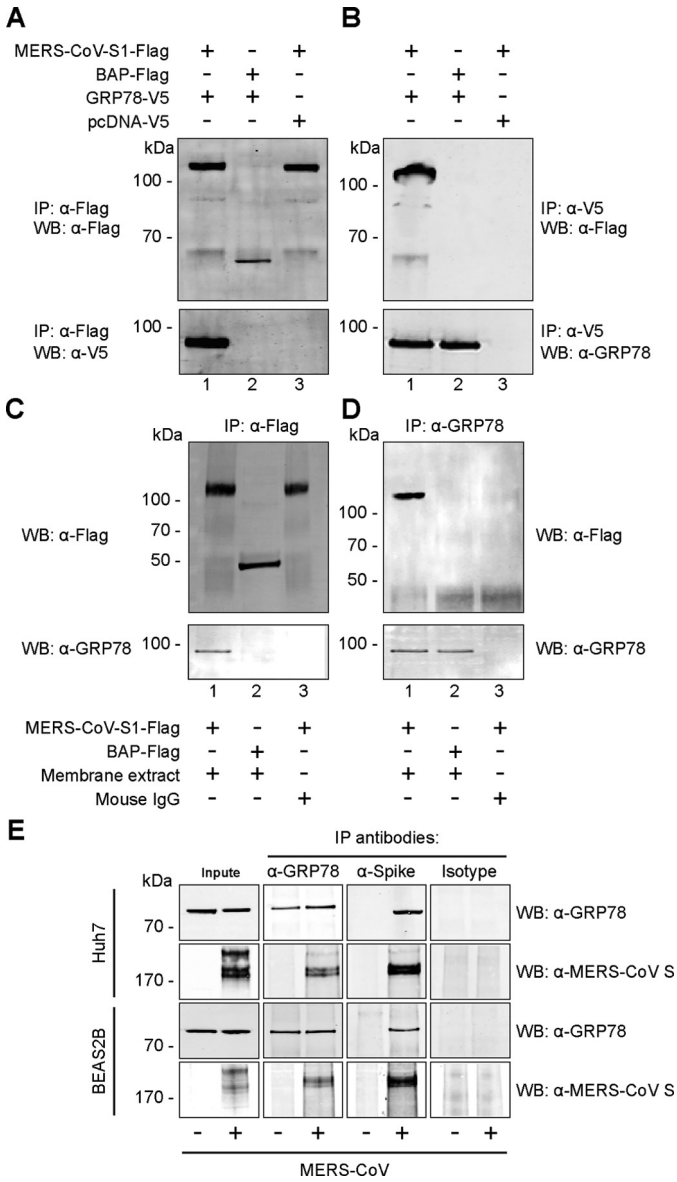

Figure 2. GRP78 interacts with the MERS-CoV spike. *A,* BHK21 cells were transfected with pcDNA–GRP78–V5 (*lanes 1* and *2*) or empty vector (*lane 3*). The cell lysate was immunoprecipitated (*IP*) with either purified recombinant MERS-CoV–S1–FLAG protein (*lanes 1* and *3*) or *E. coli* bacterial alkaline phosphatase (*BAP*)-FLAG protein (*lane 2*) pre-adsorbed onto anti-FLAG M2-agarose beads. The precipitated protein complex was detected using the anti-FLAG antibody or the anti-V5 antibody. *B,* reciprocal co-IP was performed using GRP78 as the bait protein. Purified MERS-CoV–S1–FLAG (*lanes 1* and *3*) or BAP–FLAG proteins (*lane 2*) were immunoprecipitated with overexpressed GRP78–V5 or pcDNA–V5 proteins pre-adsorbed on anti-V5 Sepharose beads. The precipitated protein complex was detected using the anti-FLAG antibody or the anti-GRP78 antibody. *C,* membrane fraction of Huh7 cells was extracted and immunoprecipitated with either MERS-CoV–S1–FLAG(*lanes 1* and *3*) or BAP–FLAG (*lane 2*). *D,* reciprocal co-IP was performed using GRP78 as the bait. Mouse IgG was used in place of the membrane extract as a negative control. *E,* endogenous co-IP was performed in MERS-CoV- or mock-infected Huh7 and BEAS2B cells. Immunoprecipitation was performed using the anti-GRP78 antibody, the anti-MERS-CoV spike antibody, or the mouse isotype control. The precipitated protein complexes were detected with the anti-MERS-CoV spike antibody or the anti-GRP78 antibody. *WB*, Western blotting.

GRP78 is abundantly expressed on the surface of human and animal cells

GRP78 is a highly conserved protein that is traditionally described as an ER-residing chaperone and plays key roles in

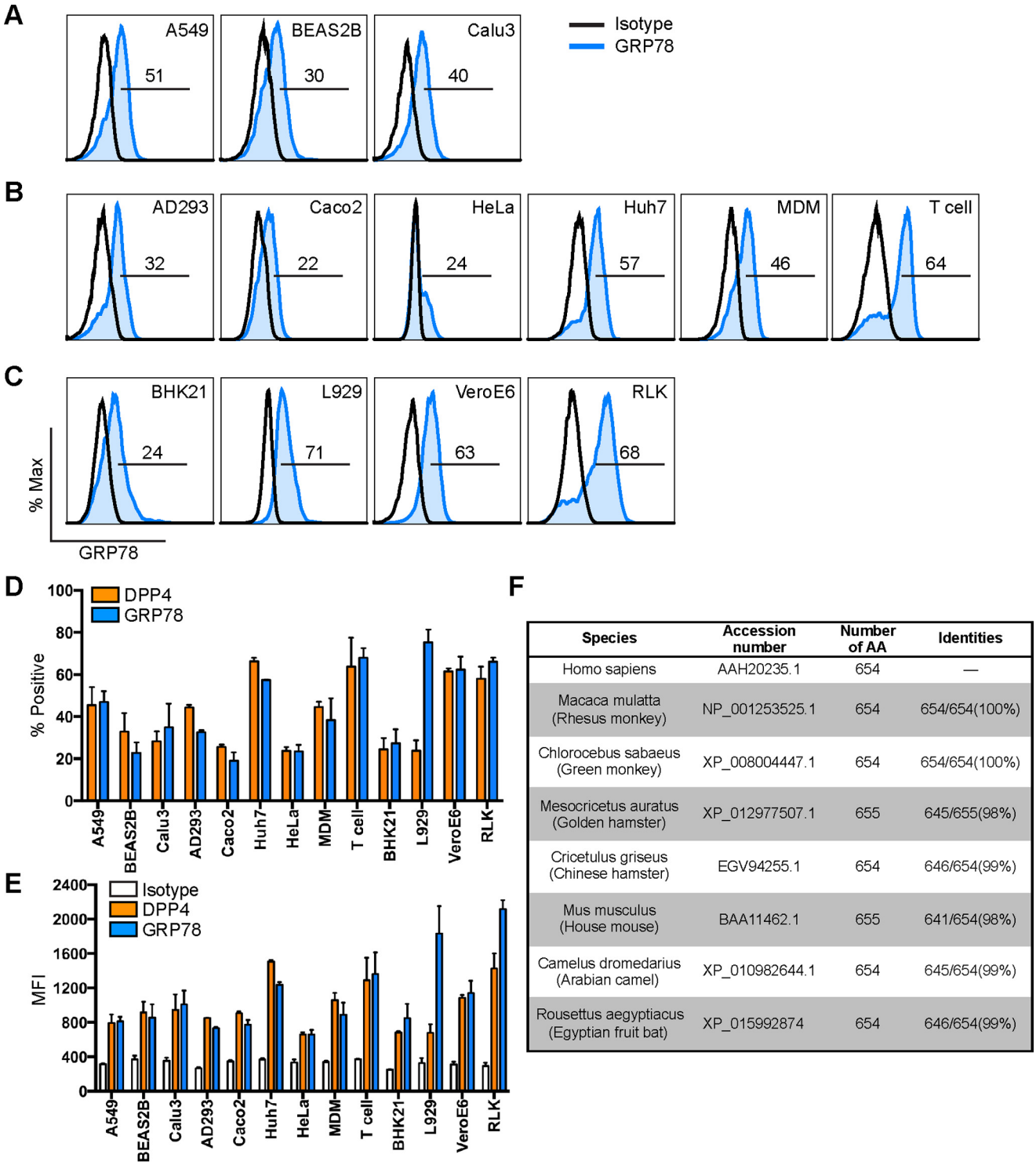

F

Species	Accession number	Number of AA	Identities
Homo sapiens	AAH20235.1	654	—
Macaca mulatta (Rhesus monkey)	NP_001253525.1	654	654/654(100%)
Chlorocebus sabaeus (Green monkey)	XP_008004447.1	654	654/654(100%)
Mesocricetus auratus (Golden hamster)	XP_012977507.1	655	645/655(98%)
Cricetulus griseus (Chinese hamster)	EGV94255.1	654	646/654(99%)
Mus musculus (House mouse)	BAA11462.1	655	641/654(98%)
Camelus dromedarius (Arabian camel)	XP_010982644.1	654	645/654(99%)
Rousettus aegyptiacus (Egyptian fruit bat)	XP_015992874	654	646/654(99%)

Figure 3. GRP78 is abundantly expressed on the cell surface of mammalian cells. Surface GRP78 expression was detected on mammalian cell lines with flow cytometry with no cell permeabilization. The immunostaining was performed for human lung cell lines (*A*), human extrapulmonary cell lines, human primary macrophages, and human primary T cells (*B*), as well as nonhuman cell lines (*C*). *D*, percentage of GRP78-positive cells quantified with DPP4 included for comparisons. *E*, MFI of GRP78 on the cell surface was quantified with isotype and DPP4 staining included as controls. *F*, sequence homology between human GRP78 and GRP78 in other mammals. Gates in *A–C* represented the percentage of GRP78-positive cells. Data in *D* and *E* represented mean and standard deviation from three independent experiments.

facilitating protein folding and assembly as well as the regulation of ER stress (28). In recent years, multiple functions of GRP78 on the cell surface have been reported, including a critical role of cell-surface GRP78 on virus entry (29–31). Because our earlier data suggested that the MERS-CoV spike could interact with plasma membrane GRP78, we hypothesized that GRP78 might be involved in modulating MERS-CoV entry or attachment. To this end, we first analyzed GRP78 expression on the cell surface of human lung cell lines that are susceptible to MERS-CoV infection (32, 33). As illustrated in Fig. 3*A*, GRP78

was readily detected on the cell surface of human lung cell lines, including A549, BEAS2B, and Calu3. In addition, GRP78 expression was also observed on the cell surface of a broad array of human cell lines (AD293, Caco2, HeLa, and Huh7) and primary cells (monocyte-derived macrophage (MDM), T cell) of extrapulmonary origin (Fig. 3*B*). Intriguingly, surface GRP78 expression was similarly detected in nonhuman cell lines, including BHK21, L929, VeroE6, and RLK. Quantitative analysis of the expression rate (Fig. 3*D*) and mean fluorescent intensity (MFI) (Fig. 3*E*) from the immunolabeled cells revealed that surface DPP4 and GRP78 were expressed at comparative levels in most measured cell lines with the exception of L929. The ubiquitous detection of GRP78 across cell lines from different species by the human GRP78 antibody could be attributed to the high degree of GRP78 sequence homology between mammalian species, suggesting that the protein is well conserved in mammalian cells (Fig. 3*F*). Altogether, the surface expression of GRP78 on MERS-CoV–susceptible cells supported the notion that GRP78 might be involved in modulating MERS-CoV entry. However, the ubiquitous expression of GRP78, particularly on cells that are not permissive to MERS-CoV infection, including BHK21 and L929, suggested that GRP78 might play an auxiliary rather than a determining role in MERS-CoV entry.

GRP78 is co-expressed with DPP4 in human pulmonary and extrapulmonary tissues

In order for GRP78 to modulate virus entry, it must be expressed by the susceptible cells at the site of infection. To explore the potential physiological relevance of GRP78 during MERS-CoV entry, we examined the distribution of GRP78 in human lung tissues with confocal microscopy. Our immunostaining results demonstrated that GRP78 was expressed at multiple regions of the human lung tissues. In particular, specific GRP78 expression was abundantly detected on the epithelial cells of the bronchus (Fig. 4*A*), bronchiole (Fig. 4*B*), and alveolus (Fig. 4*C*). Most importantly, double immunostaining of DPP4 and GRP78 revealed extensive co-localization of DPP4 and GRP78 among the epithelial cells lining the human airways (Fig. 4, *A–C*). The co-localization between DPP4 and GRP78 on the apical side of the epithelial cells indicated the potential of GRP78 in facilitating MERS-CoV entry or attachment (Fig. 4*D*, *arrows*). Interestingly, the co-expression of DPP4 and GRP78 could also be recognized in extrapulmonary tissues, including the small intestine (Fig. S3*A*) and the kidney (Fig. S3*B*). Overall, our data demonstrated that GRP78 was co-expressed with DPP4 on physiologically relevant cell types in the human lung and could potentially be involved during MERS-CoV infection in the lower respiratory tract.

Antibody blocking or siRNA knockdown of GRP78 limits MERS-CoV entry

To investigate the functional role of cell-surface GRP78 during MERS-CoV infection, we first evaluated the capacity of GRP78 antibody in blocking the entry of MERS–S-pseudovirus. In this set of experiments, Huh7 and BEAS2B cells were pre-incubated with a rabbit polyclonal antibody against GRP78 or a nontargeting rabbit control IgG. After the pre-incubation, MERS–S-pseudoviruses were added to the cells for 1 h in the presence of the GRP78 antibody or the control IgG. At 72 h post-inoculation, the cells were lysed and incubated with luciferase substrate for the quantification of infectivity. Our results demonstrated that GRP78 antibody but not the control IgG reduced MERS–S-pseudovirus entry in both Huh7 (Fig. 5*A*) and BEAS2B cells (Fig. 5*B*) in a dose-dependent manner. In stark contrast, the entry of the control vesicular stomatitis virus glycoprotein (VSV-G)-pseudovirus in both cell lines was not inhibited by GRP78 antibody (Fig. 5, *A* and *B*). Next, we proceeded to validate the antibody blocking results using infectious MERS-CoV. To this end, Huh7 cells were pre-incubated with antibodies and subsequently infected with MERS-CoV in the presence of control IgG, GRP78 antibody, or DPP4 antibody. Our data showed that the treatment of GRP78 antibody similarly inhibited MERS-CoV entry in a dose-dependent manner (Fig. 5*C*). For further verification, we infected Huh7 and BEAS2B cells with MERS-CoV after siRNA knockdown of GRP78 or DPP4. Western blotting detection demonstrated that GRP78 knockdown did not affect DPP4 or CEACAM5 expression (Fig. 5*D*). In line with the antibody blocking results, depletion of GRP78 reduced MERS-CoV entry in both Huh7 and BEAS2B cells (Fig. 5*E*). Because CEACAM5 was expressed in Huh7 but not BEAS2B cells, our data implied that the role of GRP78 in modulating MERS-CoV entry was independent of CEACAM5 expression. To further evaluate the role of GRP78 on MERS-CoV replication, we assessed virus growth in MERS-CoV–infected BEAS2B cells after siRNA knockdown of GRP78 or DPP4. Our data demonstrated that GRP78 depletion decreased MERS-CoV replication, although to a lesser extent compared with that of DPP4 knockdown (Fig. 5, *F* and *G*). Next, we asked whether GRP78 could play a role in MERS-CoV entry in the physiologically relevant primary cells. To this end, we performed siRNA knockdown of GRP78 (Fig. 5*H*) in primary human MDM and primary human embryonic lung fibroblasts (HFL), which are both susceptible to MERS-CoV infection as reported in our previous studies (32, 34). In agreement with our results from Huh7 and BEAS2B cells, GRP78 knockdown significantly reduced virus entry (Fig. 5*I*) and replication (Fig. 5, *J* and *K*) in MDM and HFL. Collectively, with antibody blocking and siRNA knockdown, we demonstrated a significant role of GRP78 during MERS-CoV entry.

GRP78 is an attachment factor of MERS-CoV

Our earlier data supported the notion that cell-surface GRP78 was involved in MERS-CoV entry. To define the functional role of GRP78 during this process, we challenged AD293 or BHK21 cells with MERS-CoV after GRP78 overexpression. First, we sought to evaluate the capacity of GRP78 in facilitating MERS-CoV attachment. To this end, GRP78-transfected AD293 or BHK21 cells were challenged with MERS-CoV at 4 °C for 2 h. After the incubation, the cells were washed, fixed, and immunolabeled for MERS-CoV N. As illustrated in Fig. 6*A*, GRP78 overexpression significantly increased virus attachment in both AD293 and BHK21 cells. Interestingly, GRP78 overexpression appeared to induce a more substantial increase in MERS-CoV attachment in the MERS-CoV–nonsusceptible BHK21 cells than that in the MERS-CoV–susceptible AD293

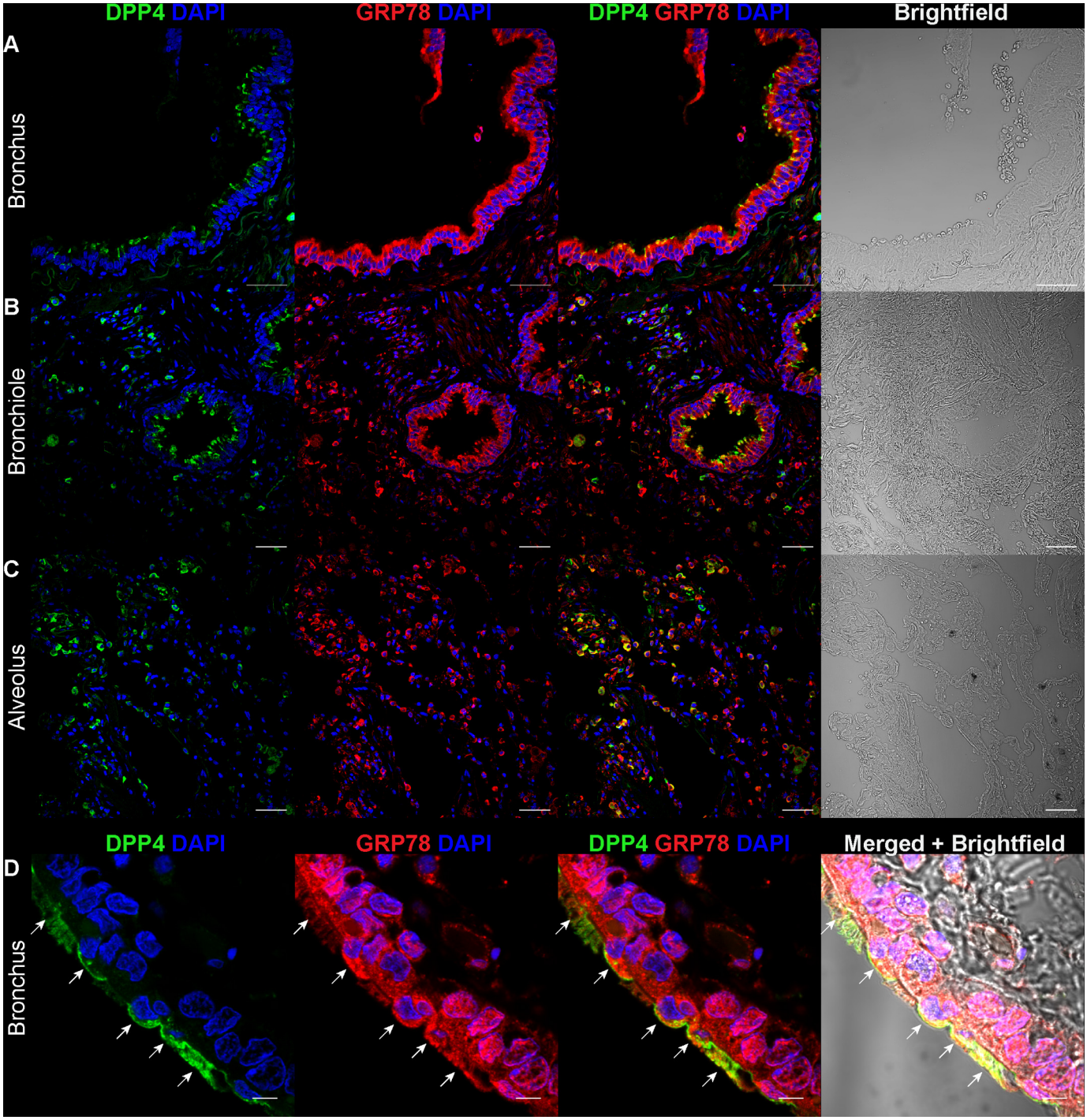

Figure 4. Co-expression of GRP78 and DPP4 in human tissues. Immunostaining of GRP78 and DPP4 was performed on paraffin slides of normal human tissues. GRP78 was labeled with a polyclonal rabbit anti-GRP78 antibody, and DPP4 was labeled with a polyclonal goat anti-DPP4 antibody. Cell nuclei were labeled with DAPI. The co-expression of GRP78 and DPP4 was detected in the bronchus (*A*), bronchiole (*B*), and alveolus (*C*). The co-localization of GRP78 and DPP4 was examined at a higher magnification in *D*. Images were acquired with a Carl Zeiss LSM 710 system. *Bars,* 50 μm for *A*–*C*. *Bars,* 5 μm for *D*.

cells (Fig. 6*B*). Next, to address whether GRP78 could independently facilitate MERS-CoV entry, we assessed the level of MERS-CoV entry in AD293 and BHK21 cells upon GRP78 overexpression. To this end, GRP78-transfected AD293 and BHK21 cells were challenged with MERS-CoV at 37 °C for 2 h. After infection, the cells were washed and incubated for another 4 h before harvesting for flow cytometry. Importantly, our result demonstrated that the nonpermissive BHK21 cells remained refractory to MERS-CoV infection despite GRP78 overexpression. In contrast, GRP78 overexpression further enhanced the entry of MERS-CoV to the permissive AD293 cells (Fig. 6, *C* and *D*). The effect of GRP78 on MERS-CoV entry was not due to ER stress (Fig. S4). Overall, our data indicated that GRP78 could not facilitate MERS-CoV entry independently but could serve as an attachment factor and modulate MERS-CoV entry in the presence of DPP4.

GRP78 is up-regulated on the surface of MERS-CoV–infected cells

Because infections by certain coronaviruses, including infectious bronchitis virus and SARS-CoV, are known to induce ER stress (35–39), which can promote GRP78 expression on the cell surface (40–43), we asked whether MERS-CoV infection could up-regulate GRP78 expression on the cell surface. To address this question, we infected Huh7 cells with MERS-CoV (Fig. 7, *A* and *B*) and harvested samples for flow cytometry at 24 h post-infection. Our result demon-

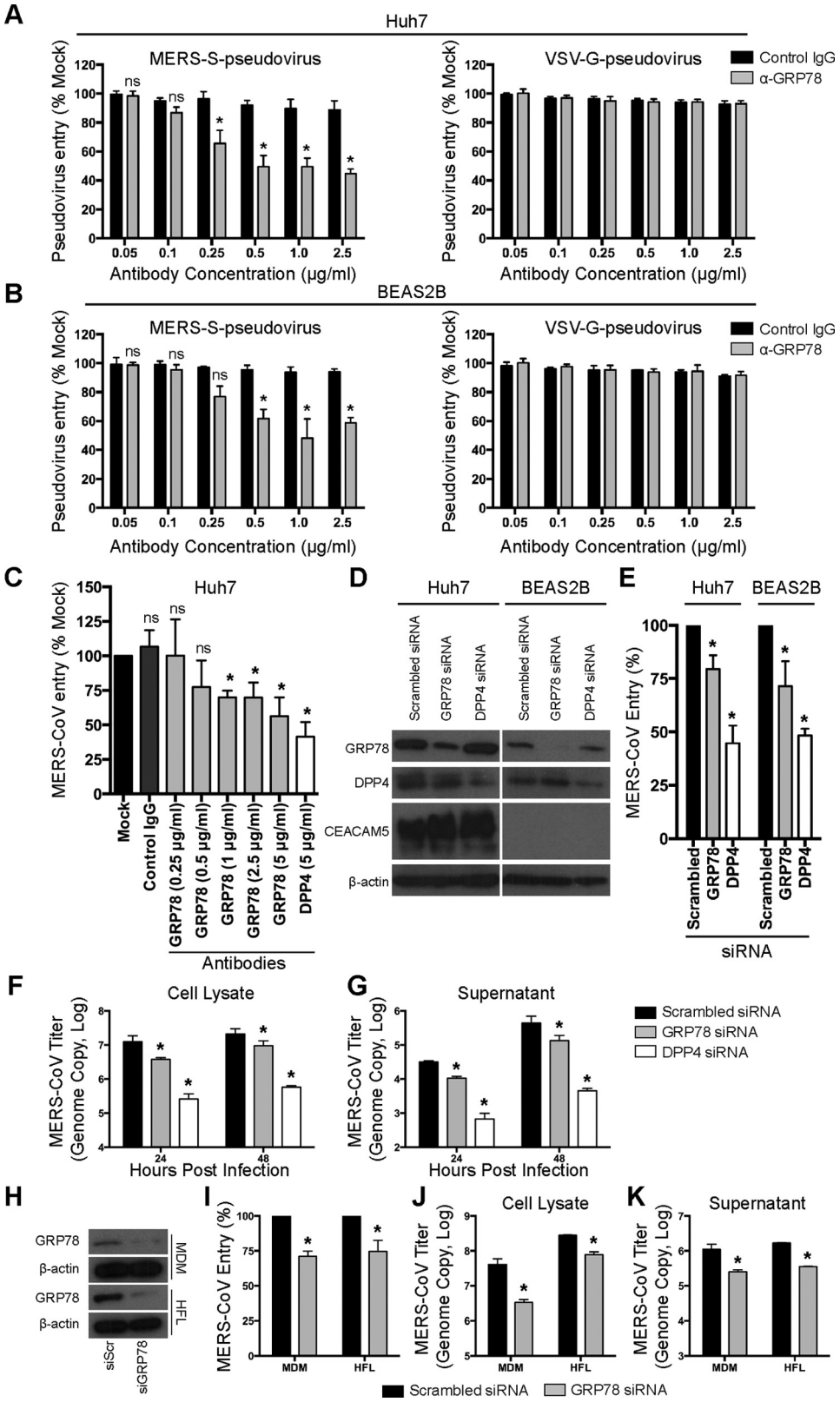

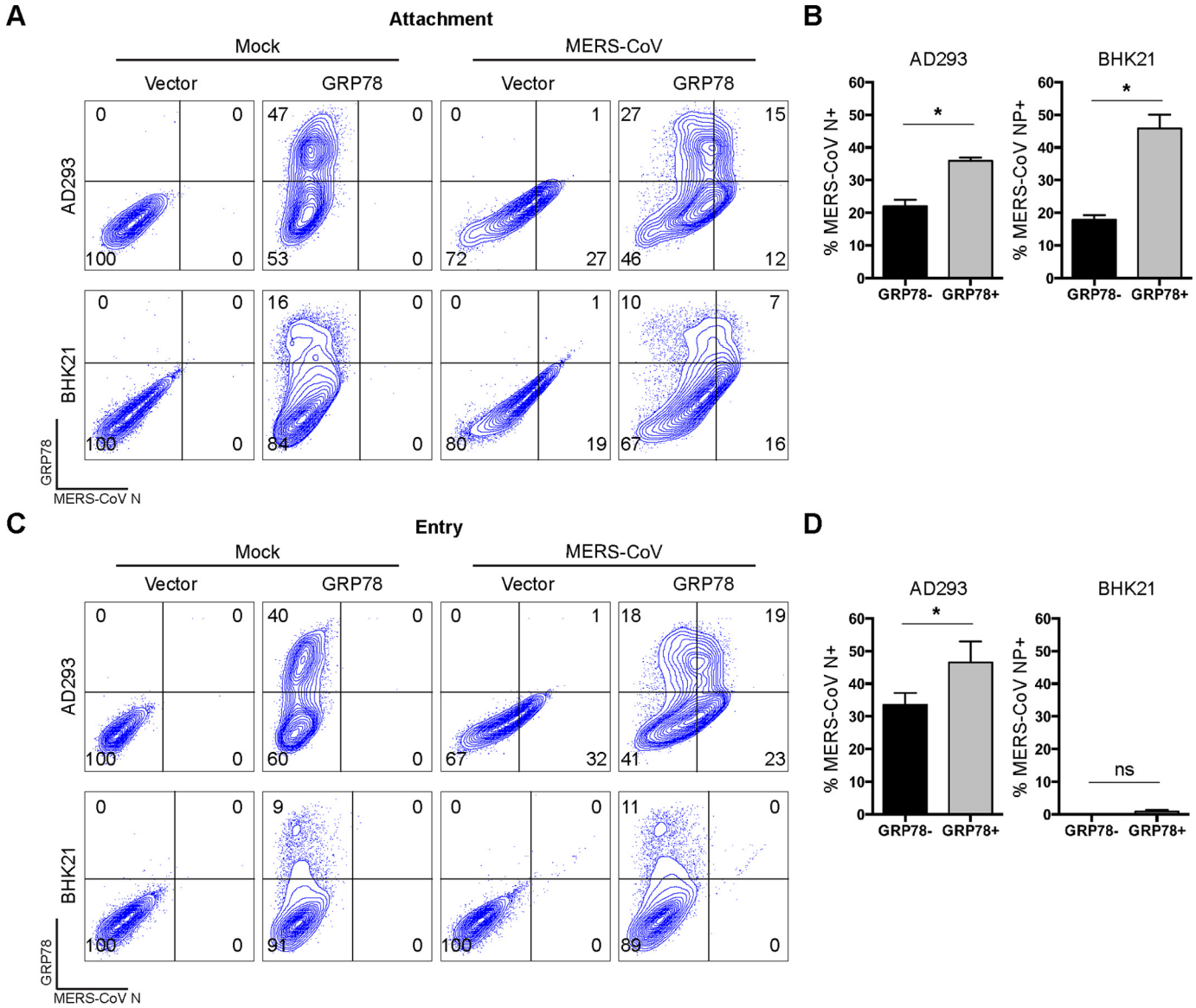

Figure 6. GRP78 is an attachment factor of MERS-CoV. *A,* to assess the role of GRP78 on MERS-CoV attachment, GRP78-overexpressing AD293 and BHK21 cells were challenged with MERS-CoV at 15 m.o.i. for 2 h at 4 °C. After 2 h, the cells were washed, detached with 10 mM EDTA on ice, and fixed in 4% paraformaldehyde before immunolabeling for flow cytometry. *B,* percentage of MERS-CoV N–positive AD293 and BHK21 cells was quantified for MERS-CoV attachment. *C,* to assess the role of GRP78 on MERS-CoV entry, GRP78-overexpressing AD293 and BHK21 cells were challenged with MERS-CoV at 5 m.o.i. for 2 h at 37 °C. After 2 h, the inoculum was replaced with culture media, and the cells were incubated for another 4 h before harvesting for flow cytometry. *D,* percentage of MERS-CoV N–positive AD293 and BHK21 cells was quantified for MERS-CoV entry. *B* and *D*, percentage of MERS-CoV N–positive cells among GRP78-transfected ($GRP78^+$) cells was calculated as (%$GRP78^+N^+$ cells/(%$GRP78^+N^+$ cells + %$GRP78^+N^-$ cells)) × 100%. The percentage of MERS-CoV N–positive cells among GRP78-nontransfected ($GRP78^-$) cells was calculated as (%$GRP78^-N^+$ cells/(%$GRP78^-N^+$ cells + %$GRP78^-N^-$ cells)) × 100%. Data represented mean and S.D. derived from three independent experiments. Statistical analyses were carried out using Student's *t* test. Statistical significance was indicated by *asterisks* when $p < 0.05$. *ns* means not significant.

Figure 5. GRP78 is involved in MERS-CoV entry. Pseudovirus antibody blocking assays were performed in Huh7 (*A*) and BEAS2B (*B*) cells. A titration of GRP78 or isotype control antibodies from 0 to 2.5 μg/ml was added and pre-incubated with Huh7 and BEAS2B cells for 1 h at 37 °C. MERS–S-pseudovirus or VSV-G–pseudovirus was subsequently added at a ratio of 100 LP per cell for 1 h. Luciferase activity was determined at 72 h post-inoculation and was normalized to that of the mock-treated cells. *C,* antibody blocking assay was performed in Huh7 cells using infectious MERS-CoV. Huh7 cells were pre-incubated with antibodies at the indicated concentration for 1 h at 37 °C. The cells were then challenged with MERS-CoV at 1 m.o.i. for 1 h at 37 °C in the presence of the antibodies. After 1 h, the cells were washed and harvested. MERS-CoV entry was assessed with qPCR, and the result was normalized to that of the mock-treated cells. *D,* Huh7 or BEAS2B cells were treated with 75 nM GRP78, DPP4, or scrambled siRNA for 2 consecutive days. The knockdown efficiency was evaluated with Western blottings. *E,* siRNA-treated Huh7 or BEAS2B cells were infected with MERS-CoV at 1 m.o.i. for 1 h at 37 °C. After 1 h, the cells were harvested, and virus entry was evaluated with qPCR analysis. The result was normalized to that of the scrambled siRNA-treated cells. siRNA-treated BEAS2B cells were infected with MERS-CoV at 0.1 m.o.i. for 1 h at 37 °C. The cell lysates (*F*) and supernatants (*G*) were harvested at 24 and 48 h post-infection. MERS-CoV replication was evaluated with qPCR analysis. *H,* siRNA-treated MDM or HFL was infected with MERS-CoV at 1 m.o.i. for 2 h at 37 °C. After 2 h, the cells were harvested, and virus entry was evaluated with qPCR analysis (*I*). The result was normalized to that of the scrambled siRNA-treated cells. siRNA-treated MDM or HFL was infected with MERS-CoV at 0.1 m.o.i. for 1 h at 37 °C. The cell lysates (*J*) and supernatants (*K*) were harvested at 24 h post-infection. MERS-CoV replication was evaluated with qPCR analysis. In all panels, data represented mean and S.D. from three independent experiments. Statistical analyses were carried out using Student's *t* test. Statistical significance was indicated by *asterisks* when $p < 0.05$. *ns* means not significant.

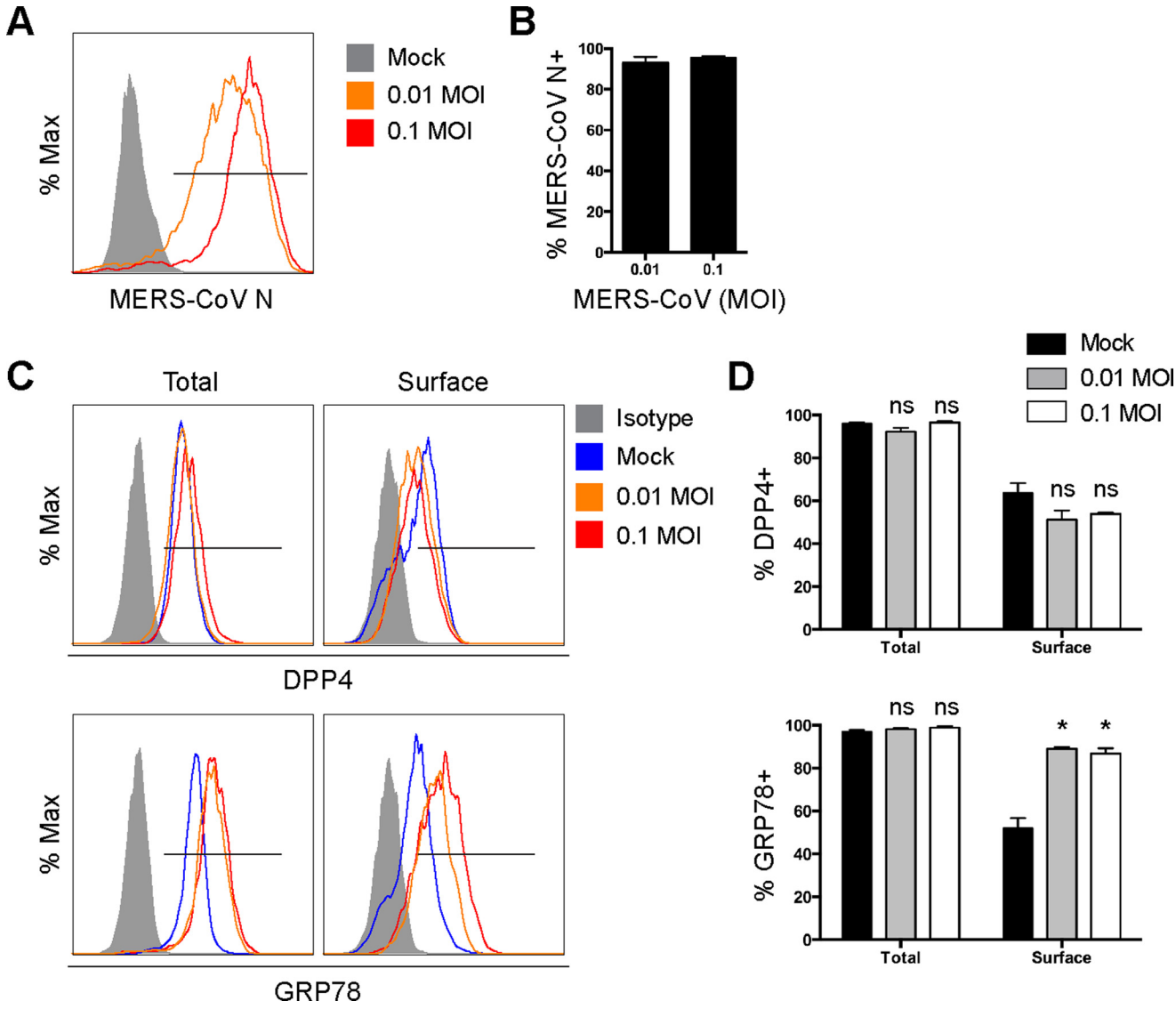

Figure 7. GRP78 is up-regulated on the surface of MERS-CoV–infected cells. *A,* Huh7 cells were infected with MERS-CoV at 0.01 and 0.1 m.o.i. and were harvested for flow cytometry analysis at 24 h post-infection. *B,* percentage of MERS-CoV N–positive cells was quantified. *C,* in parallel, cell surface and total DPP4 and GRP78 among mock- or MERS-CoV–infected samples were analyzed by flow cytometry. *D,* percentage of DPP4-positive cells and GRP78-positive cells in mock- or MERS-CoV–infected samples were quantified. Total DPP4 and GRP78 staining was performed by first permeabilizing the cells with 0.1% Triton X-100, whereas the surface DPP4 and GRP78 staining was performed in the absence of cell permeabilization. The gate in *A* represented the percentage of MERS-CoV N–positive cells. The gates in *C* represented the percentage of DPP4- (*upper panels*) and GRP78 (*lower panels*)-positive cells. Data represented mean and S.D. derived from three independent experiments. Statistical analyses were carried out using Student's *t* test. Statistical significance was indicated by *asterisks* when $p < 0.05$. *ns* means not significant.

strated that although the percentage of surface DPP4-positive cells modestly decreased after MERS-CoV infection, the percentage of surface GRP78-positive cells significantly increased from ~50 to ~80% after MERS-CoV infection (Fig. 7, *C* and *D*). In this regard, our results highlighted the potential relevance of GRP78 on MERS-CoV attachment onto the infected cells.

GRP78 facilitates the cell-surface attachment of bCoV-HKU9

Coronaviruses have evolved a complicated receptor recognition system through their spike proteins. Peculiarly, the spike proteins from highly-related coronaviruses can recognize different cell-surface molecules, whereas the spike proteins of phylogenetically distant coronaviruses can bind the same cell-surface molecule for attachment or entry (11). By exploring the potential interaction between GRP78 and the spike proteins of other coronaviruses, we unexpectedly discovered that GRP78 could interact with the spike protein of bat coronavirus HKU9 (bCoV-HKU9) (Fig. 8*A*). Interestingly, despite the capacity of binding the spike proteins of lineage C (MERS-CoV) and lineage D (bCoV-HKU9) *Betacoronavirus*, GRP78 did not interact with the spike protein of SARS-CoV, which is a lineage B *Betacoronavirus* (Fig. 8*B*). In 2007, we reported the first discovery and genome characterization of bCoV-HKU9, which was identified from Leschenault's rousette bats (*R. leschenaulti*) (44). Recently, with structural analysis and surface plasmon resonance assay, it appeared that the receptor-binding domain of bCoV-HKU9 spike was incapable of reacting with either human DPP4 or ACE2 (45). In this regard, it would be important to explore the potential physiological relevance of the interaction

between GRP78 and bCoV-HKU9 spike. We first evaluated the cell tropism of HKU9–S-pseudovirus with MERS–S-pseudovirus included as a control. Remarkably, our data suggested that among the 10 evaluated mammalian cell lines, HKU9–S-pseudovirus entry was most pronounced in *R. leschenaulti* kidney (RLK) cells (Fig. 8*C*). Notably, although MERS–S-pseudovirus entry was evident in RLK cells, culture for bCoV-HKU9 in RLK or other cell lines has not been successful (44). In line with the pseudovirus entry result, the surface-binding efficiency of HKU9–S-pseudovirus on RLK cells was ~3-fold that on Caco2 cells (Fig. 8*D*), which is a human colon cell line known to be permissive for both MERS-CoV and SARS-CoV infection. Notably, overexpression of human GRP78 in the apparently nonpermissive L929 and BHK21 cells did not render the cells permissive to HKU9–S-pseudovirus entry, indicating that GRP78 could not function as an independent receptor for bCoV-HKU9 (Fig. 8*E*). In contrast, with a flow cytometry-based surface-binding assay, we demonstrated that the GRP78 anti-

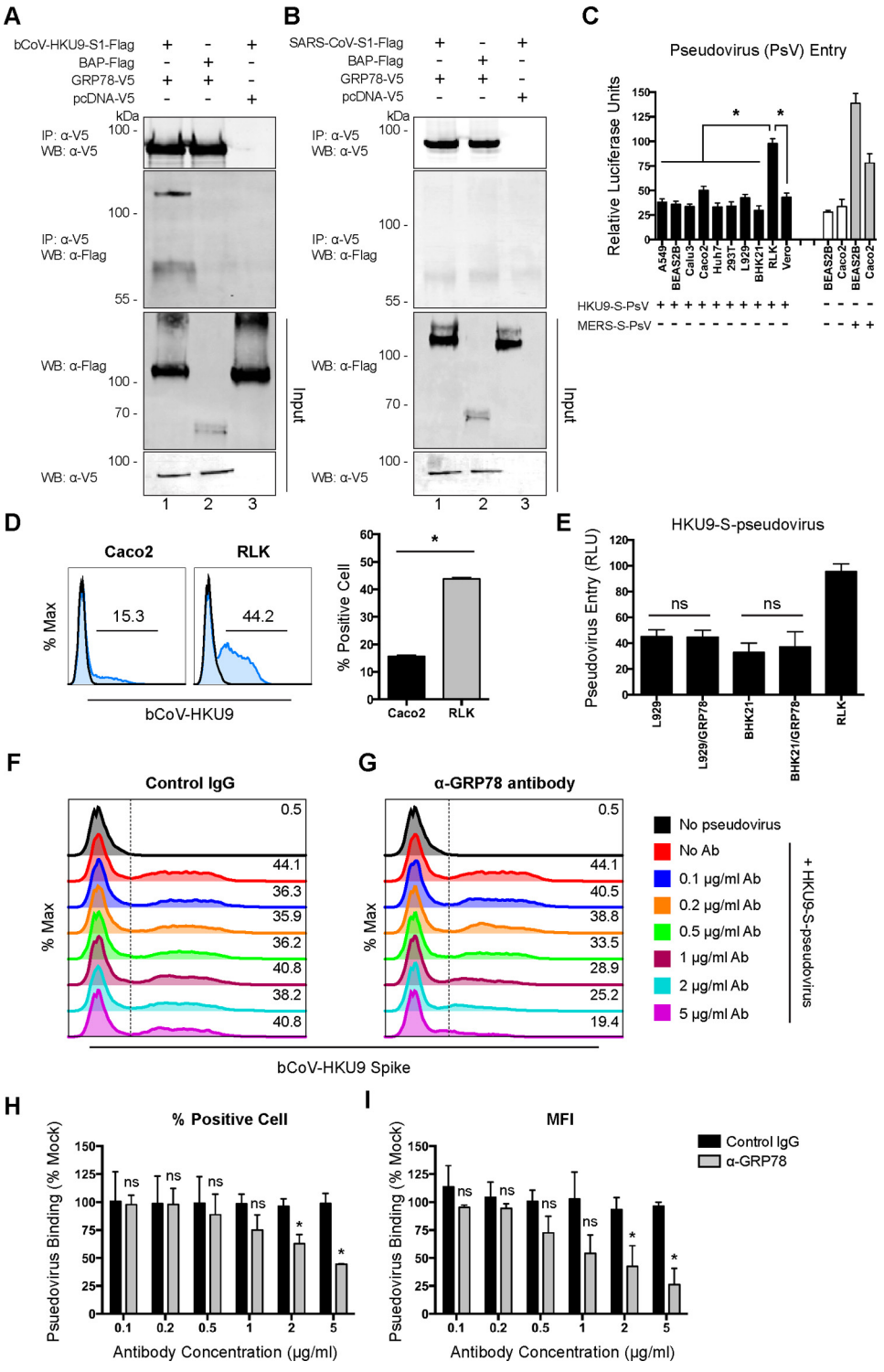

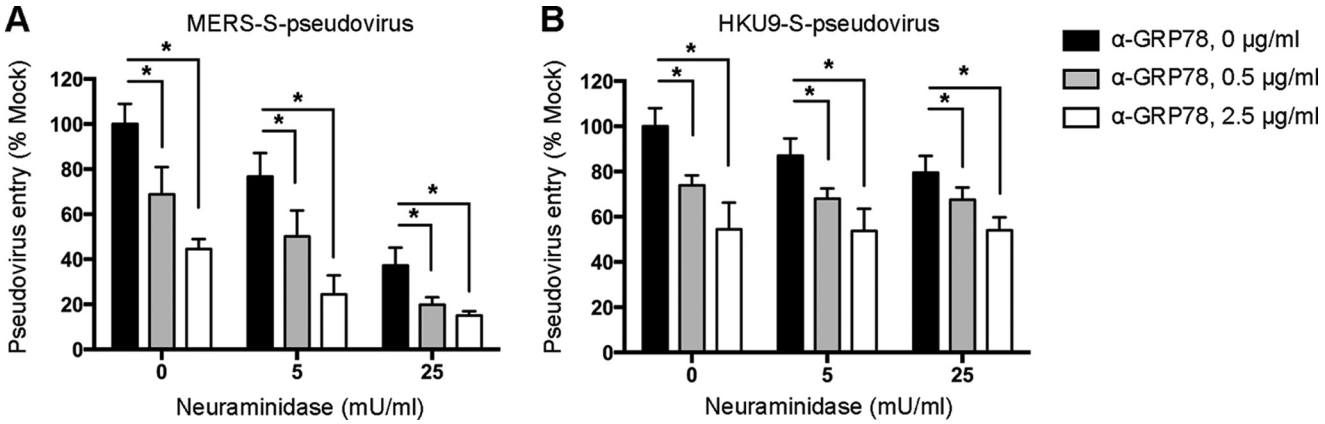

Figure 9. Sialic acids and GRP78 act independently to facilitate the surface attachment of MERS-CoV. *A,* Huh7 cells were treated with neuraminidase from *C. perfringens*, with or without pre-incubation with the GRP78 polyclonal antibody. The cells were subsequently challenged with MERS–S-pseudovirus and assessed at 72 h post-infection for pseudovirus entry. *B,* RLK cells were treated with neuraminidase from *Clostridium perfringens*, with or without pre-incubation with the GRP78 polyclonal antibody. The cells were subsequently challenged with HKU9–S-pseudovirus and assessed at 72 h post infection for pseudovirus entry. Pseudovirus entry was quantified using a microplate reader as relative light units (*RLU*). Data represented mean and standard deviation derived from three independent experiments. Statistical analyses were carried out using Student's *t* test. Statistical significance was indicated by *asterisk* marks when $p < 0.05$.

body (Fig. 8*G*) but not the control IgG (Fig. 8*F*) reduced the binding of HKU9–S-pseudovirus to the cell surface of RLK cells in a dose-dependent manner, which was evidenced by the drop in the percentage of HKU9–S-positive cells (Fig. 8*H*) as well as the decrease in the HKU9–S-mean fluorescent intensity (Fig. 8*I*). Taken together, our data identified GRP78 as an important cell surface–binding protein for both MERS-CoV and bCoV-HKU9 by serving as an attachment factor.

Sialic acids and GRP78 act independently to facilitate the surface attachment of MERS-CoV

Sialic acids were recently identified as an attachment determinant of MERS-CoV (46). To investigate whether GRP78 and sialic acids could act in conjunction with each other in facilitating the attachment of MERS-CoV, we assessed MERS–S-pseudovirus entry in the presence of a combination of neuraminidase treatment and GRP78 antibody blocking. Our results demonstrated that although neuraminidase treatment decreased MERS–S-pseudovirus entry in a dose-dependent manner, the addition of GRP78 antibody further enhanced the inhibitory effect (Fig. 9*A*). However, the entry of HKU9–S-pseudovirus was inhibited by GRP78 antibody but not neuraminidase treatment (Fig. 9*B*). Overall, the additive effect of neuraminidase treatment and GRP78 antibody on limiting MERS–S-pseudovirus entry suggested that sialic acids and GRP78 both independently facilitated the attachment of MERS-CoV onto the cell surface, whereas GRP78 but not sialic acids played an important role for virus attachment of bCoV-HKU9.

Discussion

Host tropism is predominantly determined by the interaction between coronavirus spikes and their corresponding host receptors. In addition, the spike proteins of coronaviruses can recognize a broad range of cell-surface molecules, which serve to augment coronavirus attachment or entry. In this study, we identified host GRP78 as a novel interacting target of the MERS-CoV spike (Figs. 1 and 2). GRP78 was expressed on the surface of MERS-CoV–susceptible cell lines of pulmonary and extrapulmonary origin (Fig. 3). At the same time, immunostaining of human lung tissues identified abundant co-expression of DPP4 and GRP78 in the epithelial cells along the human airways (Fig. 4). Next, with antibody blocking and siRNA knockdown experiments, our data indicated the involvement of GRP78 in MERS-CoV entry (Fig. 5). Overexpression assays of GRP78 in MERS-CoV–permissive and MERS-CoV–nonper-

Figure 8. GRP78 interacts with the bCoV-HKU9 spike and serves as an attachment factor for bCoV-HKU9. *A,* BHK21 cells were transfected with pcDNA–GRP78–V5 (*lanes 1* and *2*) or empty vector (*lane 3*). Co-IP between GRP78 and bCoV-HKU9 spike was performed using GRP78 as the bait protein. Purified bCoV–HKU9–S1–FLAG (*lanes 1* and *3*) or BAP–FLAG proteins (*lane 2*) were immunoprecipitated (*IP*) with overexpressed GRP78–V5 or pcDNA–V5 proteins pre-adsorbed on anti-V5–Sepharose beads. The precipitated protein complex was detected using the anti-V5 antibody or the anti-FLAG antibody. *B,* co-IP between GRP78 and SARS-CoV spike was performed using GRP78 as the bait protein. Purified SARS-CoV–S1–FLAG (*lanes 1* and *3*) or BAP–FLAG proteins (*lane 2*) were immunoprecipitated with overexpressed GRP78–V5 or pcDNA–V5 proteins pre-adsorbed on anti-V5–Sepharose beads. The precipitated protein complex was detected using the anti-V5 antibody or the anti-FLAG antibody. *C,* HKU9–S-pseudovirus entry assays were performed in a number of mammalian cell lines. Mock-inoculated and MERS–S-pseudovirus–inoculated cells were included as negative and positive controls, respectively. HKU9–S-pseudovirus and MERS–S-pseudovirus were added at a ratio of 100 LP per cell for 1 h. Luciferase activity was determined at 72 h post-inoculation. *D,* HKU9–S-pseudovirus attachment efficiency was evaluated in Caco2 and RLK cells. HKU9–S-pseudovirus was inoculated on Caco2 and RLK cells at 100 LP per cell for 2 h at 4 °C. After 2 h, the cells were washed, fixed, and immunolabeled for flow cytometry. HKU9–S-pseudovirus binding was identified with an in-house mouse bCoV-HKU9 spike immune serum. *E,* HKU9–S-pseudovirus entry in L929 and BHK21 cells was assessed with or without GRP78 overexpression. HKU9–S-pseudovirus was inoculated at 100 LP per cell for 1 h at 37 °C. Luciferase activity was determined at 72 h post-inoculation. *F* and *G,* antibody-blocking assay for HKU9–S-pseudovirus binding was performed in RLK cells. RLK cells were pre-incubated with the rabbit anti-GRP78 antibody and the rabbit control IgG from 0 to 5 μg/ml. After the pre-incubation, HKU9–S-pseudovirus was inoculated to the cells at 100 LP per cell for 2 h at 4 °C. The cells were then washed, fixed, and immunolabeled for flow cytometry. HKU9–S-pseudovirus binding was identified with an in-house mouse bCoV-HKU9 spike immune serum. The percentage of bCoV-HKU9 spike-positive cells was quantified in *H,* and the MFI of the bCoV-HKU9 spike on the cell surface was quantified in *I*. Gates in *D, F,* and *G* represented the percentage of HKU9 spike-positive cells. Data represented mean and S.D. derived from three independent experiments. Statistical analyses were carried out using Student's *t* test. Statistical significance was indicated by *asterisks* when $p < 0.05$. *WB,* Western blot. *ns* means not significant.

missive cells unambiguously demonstrated that GRP78 did not independently render nonpermissive cells susceptible to MERS-CoV infection but could facilitate MERS-CoV entry in conjunction with DPP4 by serving as an attachment factor (Fig. 6). Intriguingly, GRP78 was up-regulated upon MERS-CoV infection, which might further facilitate virus attachment among the infected cells (Fig. 7). Most importantly, GRP78 was also recognized by the spike protein of a bat *Betacoronavirus*, bCoV-HKU9. Our result further indicated that GRP78 was not the functional receptor of bCoV-HKU9 but could modulate HKU9–S-pseudovirus attachment to RLK cells (Fig. 8). Simultaneous treatments of neuraminidase and GRP78 antibody blocking revealed that sialic acids and GRP78 both independently facilitated the attachment of MERS-CoV onto the cell surface, whereas virus attachment of bCoV-HKU9 was mediated by GRP78 but not sialic acids (Fig. 9). Overall, our study identified GRP78 as an attachment factor that might modulate virus entry for two phylogenetically related *Betacoronaviruses* of different lineages, MERS-CoV and bCoV-HKU9.

GRP78, also referred to as BiP or HSPA5, is traditionally recognized as an ER chaperone (27). It is involved in a wide range of physiological processes, including protein folding and assembly, translocation of newly synthesized polypeptides, degradation of misfolded proteins, as well as maintaining the ER homeostasis (27). In addition, GRP78 is an essential regulator of ER stress due to its critical role in the unfolded protein response pathway. Despite its participation in ER-related functions, GRP78 is also detected in other cellular fractions, including mitochondria, nucleus, cytosol, and plasma membrane (43). In recent years, an increasing number of studies have described the physiological role of cell-surface GRP78 during virus entry. For instance, GRP78 was identified as a co-receptor for coxsackievirus A9 (CVA9) (30) and dengue virus (47). In addition, cell-surface GRP78 also facilitates the entry of Japanese encephalitis virus (29). Here, we reported GRP78 as a host factor that could serve as an attachment protein for two *Betacoronaviruses*, MERS-CoV and bCoV-HKU9. In its capacity as an attachment factor, GRP78 may serve to concentrate virus particles on the cell surface, which may then increase the possibility of receptor-mediated virus entry for MERS-CoV and bCoV-HKU9. Importantly, MERS-CoV infection resulted in an up-regulation of GRP78 on the cell surface, which may in turn increase the attachment of MERS-CoV and further enhance the possibility of virus entry in the infected cells.

Coronaviruses can recognize a wide range of cell-surface molecules, including cell membrane proteins and sugars in addition to their cellular receptors. As an example, HCoV-NL63 employs ACE2 for host cell entry (14) but can bind to cell-surface heparan sulfate proteoglycans to enhance attachment and infection of target cells (16). We have previously reported the identification of CEACAM5 as an attachment factor of MERS-CoV, which could facilitate MERS-CoV entry in the presence of DPP4 (25). Recently, CD9 was reported as a host factor that could augment MERS-CoV entry by bringing the cellular receptor and proteases into close proximity, thus increasing the infection efficiency (26). In this study, the identification of GRP78 as an attachment factor of MERS-CoV further indicated that the spike protein of MERS-CoV is highly efficient in engaging multiple cell surface factors to facilitate virus entry. In contrast to CEACAM5, which is expressed on limited cell types (25), surface GRP78 expression appeared to be relatively abundant across various cell types of different tissue origin (Fig. 3). In addition, a remarkable level of GRP78 was specifically detected on the epithelial cells along the human airways, where it was found to colocalize with DPP4 (Fig. 4). In this regard, it is tempting to speculate that the capacity of the MERS-CoV spike to utilize multiple host surface proteins, including CEACAM5, CD9, and GRP78, may give MERS-CoV a physiological advantage in establishing efficient infections, which may contribute to the high pathogenicity of the virus.

Bat coronavirus HKU9 (bCoV-HKU9) is a representative lineage D *Betacoronavirus*. The virus was first identified in 2007 in a territory-wide molecular surveillance study on bat samples from the Guangdong province of Southern China (44). Subsequent studies suggested that the virus was widely distributed and was circulating in different bat species (48–51). Structural and functional features of the receptor-binding domain (RBD) of bCoV-HKU9 demonstrated that the spike protein of the virus was incapable of interacting with either DPP4 or ACE2 (45). However, the RBD of bCoV-HKU9 contained a conserved core structure that was shared across other *Betacoronaviruses*, including MERS-CoV, SARS-CoV, and bat coronavirus HKU4 (bCoV-HKU4) (45). Notably, recent reports demonstrated that bCoV-HKU4 could recognize human DPP4 as a functional receptor, indicating the potential of bat coronaviruses in human adaptations. In this regard, the identification of GRP78 as a shared attachment factor for MERS-CoV and bCoV-HKU9 is interesting but alarming, which highlighted the importance of continuous surveillance on the other members of the *Betacoronavirus* genus for their capacity of interspecies transmission.

In summary, almost all presently circulating human coronaviruses have a phylogenetically-related virus partner found in animals. The human *Alphacoronavirus* HCoV-NL63 may be a recombinant between NL63-like viruses in *Triaenops* bats and 229E-like viruses circulating in *Hipposideros* bats (52). Another human *Alphacoronavirus* HCoV-229E has closely-related 229E-like coronaviruses recently isolated from dromedary camels (53). Similarly, the lineage A *Betacoronavirus* HCoV-OC43 was postulated to originate from a bovine coronavirus and jumped into human in the 1890s (2, 54). The lineage B *Betacoronavirus*, SARS-CoV, originated from either civets or bats, which jumped into human in 2003 (55, 56), whereas the lineage C *Betacoronavirus*, MERS-CoV, is likely to have jumped from camels into human in 2012 (57, 58). Because three (lineages A, B, and C) out of four lineages of animal *Betacoronaviruses* have independently jumped from animal into human in the recent past, there is enough reason to suspect that a lineage D *Betacoronavirus* may also jump into human one day. Our finding of the lineage C MERS-CoV and lineage D bCoV-HKU9 sharing the same host attachment factor GRP78 highlights the importance of monitoring the evolution of bCoV-HKU9, which may jump the interspecies barrier into human leading to another major epidemic in the future.

Experimental procedures

Cells

A549, AD293 (a derivative of the commonly used HEK293 cell line, with improved cell adherence), HeLa, Huh7, Caco2, and VeroE6 cells were maintained in Dulbecco's modified Eagle's medium (DMEM) supplemented with 10% heat-inactivated fetal bovine serum (FBS), 100 units/ml penicillin, and 100 μg/ml streptomycin. BEAS2B (transformed epithelial cells isolated from normal human bronchial epithelium) and Calu3 cells were maintained in supplemented DMEM/F-12. BHK21, L929, RLK, and HFL were maintained in supplemented minimum essential medium. Human primary monocytes were obtained from human peripheral blood mononuclear cells (PBMCs) as described previously (59). Primary human monocyte-derived macrophages (MDMs) were differentiated from monocytes in Roswell Park Memorial Institute (RPMI)-1640 media supplemented with 10% FBS, 100 μg/ml streptomycin, 100 units/ml penicillin, 2 mM glutamine, 1% sodium pyruvate, 1% nonessential amino acids, and 10 ng/ml recombinant human granulocyte macrophage colony-stimulating factor (GM-CSF) (R&D Systems) (60). Human primary T cells were isolated from PBMCs with negative selection using the Dynabeads Untouched Human T cells kit (Invitrogen) as we described previously (61). Isolated T cells were maintained in RPMI 1640 medium supplemented with 10% FBS, 100 μg/ml streptomycin, 100 units/ml penicillin, 1% sodium pyruvate, and 1% nonessential amino acids.

Virus

MERS-CoV was a gift from Dr. Ron Fouchier (Erasmus Medical Center, Rotterdam, the Netherlands) and cultured in VeroE6 cells in serum-free DMEM. Virus titers were quantified with plaque assays as described previously (25).

Antibodies

MERS-CoV nucleocapsid protein (N) was detected with the in-house guinea pig anti-MERS–CoV N serum as we described previously (32, 62). The MERS-CoV spike was detected with either the in-house mouse anti-MERS-CoV spike immune serum or a rabbit anti-MERS-CoV spike antibody from Sino Biological (40069-RP02). An in-house mouse anti-bCoV-HKU9-spike immune serum was used to detect bCoV-HKU9 spike. Primary antibodies, including rabbit anti-DPP4 (ab28340), rabbit anti-GRP78 (ab21685), rabbit anti-pan-cadherin (ab16505), rabbit anti-calreticulin (ab2907), rabbit anti-GM130 (ab52649), rabbit anti-EGFR (ab52894), and rabbit anti-CEACAM5 (ab131070), were from Abcam. Rabbit anti-lamin A was from Sigma (SAB4501764). Rabbit control IgG was from ThermoFisher Scientific (31235). Mouse anti-GRP78 antibody for Western blotting was from R&D Systems (MAB4846). Rabbit anti-GRP78 from Novus Biologicals (NBP1-54318) and goat anti-CD26 from R&D Systems (AF1180) were used for antibody-blocking experiments. Rabbit anti-giantin was from Biolegend (A488-114L). The mouse anti-β-actin was from Sigma (A5441). The recombinant FLAG-conjugated proteins were detected with an anti-FLAG M2 antibody from Sigma (F1804). The V5-tagged proteins were detected with mouse anti-V5 antibodies from Immnoway (YM3005) or ThermoFisher Scientific (R96025). The eGFP-tagged proteins were detected with a rabbit anti-eGFP from Abcam (ab290). Secondary antibodies, including Alexa Fluor 488/647 goat anti-guinea pig (A11073/A21450) and Alexa Fluor 488/647 goat anti-rabbit (A11008/A21245) from ThermoFisher Scientific, were used for flow cytometry. The goat anti-mouse HRP (626520) and goat anti-rabbit HRP (656120) antibodies from ThermoFisher Scientific were used for Western blottings.

Plasmid construction

The construction of pcDNA–MERS–CoV–S was previously described (25). Codon-optimized bCoV-HKU9-spike DNA was synthesized at GeneArt (ThermoFisher Scientific) based on amino acid sequence of the bCoV-HKU9 (44) and cloned into the pcDNA3.1(+) vector. In parallel, bCoV-HKU9–S1 was subcloned into the pSFV1 vector with a FLAG sequence in-frame in the 3′-end for protein expression. The expression construct for codon-optimized SARS-CoV spike, pcDNA-Sopt9, was a gift from Dr. Chen Zhiwei and was previously described (63). The construction of pSFV–MERS-CoV–S1–FLAG was previously described (25). The same ORF was PCR-amplified and subcloned into pcDNA3.1(+) vector in-frame with a V5 epitope, which resulted in pcDNA–MERS-CoV–S1–V5. The GRP78-coding region, including the N-terminal signal peptide, was obtained with RT-PCR from BEAS2B cells and cloned into pcDNA3.1(+) vector fused with V5, which resulted in pcDNA–GRP78–V5.

Immunoaffinity purification of MERS-CoV–S1–FLAG protein

Expression of FLAG-tagged recombinant proteins was previously described (64, 65). In brief, linearized pSFV–FLAG plasmids were transcribed *in vitro,* and the derived capped RNAs were electroporated into BHK21 cells. At 15 h post-transfection, the cells were lysed, and the expressed recombinant proteins were immunopurified using anti-FLAG M2– coated beads (Sigma) according to the manufacturer's instructions. The purified S protein was assessed by SDS-PAGE and Western blotting. Protein concentration was quantified with the Pierce BCA assay (ThermoFisher Scientific).

Membrane extraction

pcDNA–MERS-CoV–S1–V5–transfected BEAS2B cells cultured in 10-cm dishes were harvested by scraping cells into HEPES solution (10 mM HEPES, pH 7.5, 1.5 mM $MgCl_2$, 1 mM KCl) and centrifuging briefly at 500 $\times$ *g* for 3 min. Cell pellets were then homogenized in membrane lysis buffer (20 mM Tris-HCl, pH 7.5, 150 mM NaCl, 1% Nonidet P-40 (Calbiochem), 1% *n*-dodecyl β-maltoside (ThermoFisher Scientific), 5% glycerol, pH 7.5, with protease inhibitor mixture (Roche Applied Science)) and incubated on ice for 30 min. Residual cellular debris and nuclei in the resulting extracts were sedimented by centrifugation at 4 °C for 5 min at 6000 $\times$ *g*. The solubilized membrane proteins in the supernatant were transferred and subjected to an additional spin at 16,000 $\times$ *g* for 30 min at 4 °C, and the membrane extracts were then resuspended in lysis buffer. All extracts were quantitated using the Pierce

BCA assay kit (ThermoFisher Scientific) and stored in aliquots at −80 °C until used.

Identification of GRP78 by immunoprecipitation and MS

Membrane proteins from pcDNA–MERS-CoV–S1–V5–transfected BEAS2B cells were immunoprecipitated with mAb against V5 (ThermoFisher Scientific, R96025) and Sepharose A/G beads (ThermoFisher Scientific). In parallel, the membrane proteins from the BEAS2B cells were immunoprecipitated with purified MERS-CoV–S1–FLAG protein, anti-FLAG M2 antibody (Sigma, F1804), and Sepharose A/G beads (ThermoFisher Scientific). Pulled down proteins reactive to anti-V5 beads were washed and incubated with 0.1 M glycine, pH 3.5, and those reactive to anti-FLAG M2 beads were eluted in 3× FLAG peptide solution (Sigma, 150 ng/μl final concentration). Eluted samples were spin-dialyzed in Amicon spin column with 10-kDa cutoff (Millipore) and separated by SDS-PAGE, stained with SilverQuest kit (ThermoFisher Scientific). The gel fragment was excised for LC-MS/MS analysis carried out in the Center for Genomic Sciences, University of Hong Kong. MS/MS data were searched against all mammalian protein databases in NCBI and Swiss-Prot. The protein was identified as GRP78 with significant hits over different domains of the sequence.

Production of pseudotyped viruses

Lentivirus-based coronavirus spike pseudoviruses were generated by co-transfection of 293FT cells with the pcDNA full-length spike plasmids in combination with the HIV-1 backbone plasmid-bearing luciferase reporter gene, pNL4–3-ΔE-Luc (obtained from the AIDS Research and Reference Reagent Program) using Lipofectamine 2000 (ThermoFisher Scientific). Cells transfected overnight were replenished with fresh medium supplemented with 1 mM sodium pyruvate (ThermoFisher Scientific). Supernatants were harvested 48 h post-transfection, filtered through a 0.45-μm syringe filter, and concentrated by ultracentrifugation in 30% sucrose solution in a Beckman rotor SW32Ti at 32,000 rpm for 1 h at 4 °C. The virus pellets were resuspended in PBS, aliquoted, and stored at −80 °C. The p24 concentrations were quantified using a p24 enzyme-linked immunoassay kit (Cell BioLabs). Pseudovirus titer was quantified in units of lentiviral particle (LP) per ml according to the manufacturer's instruction.

Luciferase activity assay for pseudovirus entry

Coronavirus spike pseudoviruses were used to infect 5×10^3 target cells in white 96-well plates (Corning-Costar). After incubating the cultures for 72 h at 37 °C, the cells were first washed with PBS (ThermoFisher Scientific). The cells were then lysed with the lysis buffer (Promega) on ice, and luciferase substrate (Promega) was then added immediately. The infectivity was measured using a microplate reader (Beckman DTX880) as relative light units (RLU). Uninfected cells were included as mock controls for all experiments. All experiments were performed in triplicate and repeated at least two times.

Quantitative RT-PCR

Cells were lysed in RLT buffer with 40 mM DTT and extracted with the RNeasy mini kit (Qiagen). Viral RNA in the supernatant was extracted with the PureLink Viral RNA/DNA mini kit (Life Technologies, Inc.). Reverse transcription (RT) and quantitative PCR (qPCR) were performed with the Transcriptor First Strand cDNA synthesis kit and LightCycler 480 master mix from Roche Applied Science as we previously described (34). In the RT reactions, reverse primers against the N gene of MERS-CoV were used to detect cDNA complementary to the positive strand of viral genomes. The following sets of primers were used to detect N in qPCR: forward, 5′-CAAAACCTTCCCTAAGAAGGAAAAG-3′, reverse, 5′-GCTCCTTTGGAGGTTCAGACAT-3′, and probe (6-carboxyfluorescein), 5′-ACAAAAGGCACCAAAAGAAGAATCAACAGACC-3′ BHQ1.

Antibody-blocking assay for HKU9–S-pseudovirus binding

RLK cells were pre-incubated with the rabbit anti-GRP78 antibody (Novus Biologicals, NBP1-54318) or the rabbit control IgG (ThermoFisher Scientific, 31235) for 1 h at 37 °C. After the pre-incubation, HKU9–S-pseudoviruses were inoculated to the cells for attachment at 100 LP per cell at 4 °C for 2 h. After 2 h of incubation, the cells were washed twice with chilled PBS and fixed in 4% paraformaldehyde for 15 min. The fixed cells were immunolabeled for the bCoV-HKU9 spike with the in-house mouse bCoV-HKU9 spike immune serum and the mouse Alexa Fluor 488 goat anti-mouse secondary antibody (ThermoFisher Scientific). The binding of the HKU9–S-pseudoviruses was assessed with flow cytometry.

Antibody-blocking assay for MERS-CoV entry

Huh7 cells were pre-incubated with rabbit polyclonal anti-GRP78 (Novus Biologicals, NBP1-54318) at different concentrations ranging from 0 to 5 μg/ml. Goat polyclonal anti-DPP4 at 5 μg/ml (R&D, AF1180) and rabbit IgG at 5 μg/ml (ThermoFisher Scientific, 31235) were included as controls. After pre-incubating with the antibodies for 1 h at 37 °C, the cells were challenged with MERS-CoV at 1 m.o.i. for 1 h at 37 °C in the presence of antibodies. The cells were subsequently washed with PBS and lysed with RLT (Qiagen) with 40 mM dithiothreitol (DTT). The virus copy number was quantified with qPCR as described previously (25).

siRNA knockdown and virus entry assessment

ON-TARGETplus human GRP78 siRNA (L-008198-00-0005) and ON-TARGETplus nontargeting siRNA (L-001810-10-0020) were obtained from Dharmacon. Transfection of siRNA on BEAS2B, Huh7, MDM, or HFL cells was performed using Lipofectamine RNAiMAX (ThermoFisher Scientific) following the manufacturer's manual. In brief, the cells were transfected with 75 nM siRNA for 2 consecutive days. At 24 h after the second siRNA transfection, the cells were counted and harvested in RIPA for Western blottings. In parallel, siRNA-transfected cells were challenged with MERS-CoV at 1 m.o.i. for 1 h at 37 °C. Following the incubation, the cells were washed with PBS and lysed in RLT buffer (Qiagen) with 40 mM DTT. The virus copy number was determined with qPCR.

Neuraminidase treatment and GRP78 antibody blocking for pseudovirus entry

Huh7 and RLK cells grown in 96-well plates were washed twice with PBS (ThermoFisher Scientific) and incubated with neuraminidase from *Clostridium perfringens* (Sigma) diluted in FBS-free growth medium at 37 °C for 3 h. After the incubation, the cells were washed three times and challenged with MERS–S- or HKU9–S-pseudoviruses, with or without pre-incubation with the GRP78 polyclonal antibody (Abcam) for 1 h at 37 °C. Fresh complete medium with 10% FBS was replaced at 18 h post-infection. Pseudovirus entry was quantified using a microplate reader (Beckman DTX880) as RLU at 72 h post-infection.

Flow cytometry

Immunostaining for flow cytometry was performed following standard procedures as we previously described (61). To determine the surface-expression level of GRP78 and DPP4, the cells were detached with 10 mM EDTA in PBS, fixed in 4% paraformaldehyde, followed by immunolabeling with antibodies against GRP78 (Abcam, 21685) or DPP4 (Abcam, 28340) without cell permeabilization. For experiments with intracellular stainings, cells were detached with 10 mM EDTA in PBS, fixed in 4% paraformaldehyde, and permeabilized with 0.1% Triton X-100 in PBS. The flow cytometry was performed using a FACSCanto II flow cytometer (BD Biosciences), and data were analyzed using FlowJo version X (Tree Star).

Flow cytometry of BHK21 and AD293 cells with GRP78 overexpression

AD293 and BHK21 cells were transfected with pcDNA–GRP78–V5 with Lipofectamine 3000 (ThermoFisher Scientific). The transfected cells were inoculated with MERS-CoV at 48 h post- transfection. To determine virus entry, the cells were inoculated with MERS-CoV at 5 m.o.i. at 37 °C for 2 h. After 2 h, the cells were washed with PBS and incubated for another 4 h. At 6 h post-infection, the cells were washed extensively with PBS, fixed in 4% paraformaldehyde, and immunolabeled for flow cytometry. To determine virus attachment, the cells were inoculated with MERS-CoV at 15 m.o.i. at 4 °C for 2 h. After 2 h, the cells were washed with PBS, fixed in 4% paraformaldehyde, and immunolabeled for flow cytometry.

Confocal microscopy of human tissues

This study was approved by the Institutional Review Board of the University of Hong Kong/Hospital Authority Hong Kong West Cluster. Normal human lung sections were deparaffinized and rehydrated following standard procedures. Antigen unmasking was performed by boiling tissue sections with the antigen unmasking solution from Vector Laboratories. Goat anti-DPP4 was obtained from R&D Systems (AF1180) and rabbit anti-GRP78 was obtained from Abcam (ab21685). Cell nuclei were labeled with the DAPI nucleic acid stain from ThermoFisher Scientific (D21490). Alexa Fluor secondary antibodies were obtained from ThermoFisher Scientific. Mounting was performed with the Vectashield mounting medium (Vector Laboratories). Images were acquired with a Carl Zeiss LSM 710 system.

Statistical analysis

Data on figures represent the means and standard deviations. Statistical comparison between different groups was performed by Student's *t* test using GraphPad Prism 6. Differences were considered statistically significant when $p < 0.05$.

Author contributions—H. C., C.-M. C., J. F.-W. C., and K.-Y. Y. conceptualization; H. C., C.-M. C., X. Zhang, Y. W., S. Y., K.-H. S., D. Y., H. S., Y. H., C. L., X. Zhao, V. K.-M. P., S.-P. L., and K.-Y. Y. data curation; H. C., C.-M. C., X. Zhang, Y. W., S. Y., J. Z., R. K.-H. A.-Y., K.-H. S., D. Y., H. S., Y. H., C. L., X. Zhao, V. K.-M. P., and K.-Y. Y. formal analysis; H. C. and K.-Y. Y. supervision; H. C. and C.-M. C. validation; H. C. and C.-M. C. investigation; H. C. visualization; H. C., C.-M. C., X. Zhang, Y. W., S. Y., J. Z., R. K.-H. A.-Y., K.-H. S., D. Y., H. S., Y. H., C. L., X. Zhao, V. K.-M. P., S.-P. L., and K.-Y. Y. methodology; H. C., J. F.-W. C., and K.-Y. Y. writing-original draft; H. C., G. F. G., J. F.-W. C., and K.-Y. Y. project administration; H. C., X. Zhang, J. Z., M.-L. Y., J. Y., G. L., D.-Y. J., G. F. G., J. F.-W. C., and K.-Y. Y. writing-review and editing; R. K.-H. A.-Y., K.-H. S., M.-L. Y., J. Y., G. L., D.-Y. J., G. F. G., J. F.-W. C., and K.-Y. Y. resources; K.-H. S. software; G. F. G., J. F.-W. C., and K.-Y. Y. funding acquisition.

Acknowledgment—We thank the staff at the Core Facility, Li Ka Shing Faculty of Medicine, University of Hong Kong, for facilitation of the study.

References

1. Peck, K. M., Burch, C. L., Heise, M. T., and Baric, R. S. (2015) Coronavirus host range expansion and Middle East respiratory syndrome coronavirus emergence: biochemical mechanisms and evolutionary perspectives. *Annu. Rev. Virol.* **2,** 95–117 CrossRef Medline
2. Chan, J. F., To, K. K., Tse, H., Jin, D. Y., and Yuen, K. Y. (2013) Interspecies transmission and emergence of novel viruses: lessons from bats and birds. *Trends Microbiol.* **21,** 544–555 CrossRef Medline
3. Chan, J. F., To, K. K., Chen, H., and Yuen, K. Y. (2015) Cross-species transmission and emergence of novel viruses from birds. *Curr. Opin. Virol.* **10,** 63–69 CrossRef Medline
4. Chan, J. F., Lau, S. K., To, K. K., Cheng, V. C., Woo, P. C., and Yuen, K. Y. (2015) Middle East respiratory syndrome coronavirus: another zoonotic betacoronavirus causing SARS-like disease. *Clin. Microbiol. Rev.* **28,** 465–522 CrossRef Medline
5. Tang, J. W., Lam, T. T., Zaraket, H., Lipkin, W. I., Drews, S. J., Hatchette, T. F., Heraud, J. M., Koopmans, M. P., and INSPIRE investigators. (2017) Global epidemiology of non-influenza RNA respiratory viruses: data gaps and a growing need for surveillance. *Lancet Infect. Dis.* 17, e320–e326 CrossRef Medline
6. Chan, J. F., Li, K. S., To, K. K., Cheng, V. C., Chen, H., and Yuen, K. Y. (2012) Is the discovery of the novel human betacoronavirus 2c EMC/2012 (HCoV-EMC) the beginning of another SARS-like pandemic? *J. Infect.* **65,** 477–489 CrossRef Medline
7. Peiris, J. S., Lai, S. T., Poon, L. L., Guan, Y., Yam, L. Y., Lim, W., Nicholls, J., Yee, W. K., Yan, W. W., Cheung, M. T., Cheng, V. C., Chan, K. H., Tsang, D. N., Yung, R. W., Ng, T. K., *et al.* (2003) Coronavirus as a possible cause of severe acute respiratory syndrome. *Lancet* **361,** 1319–1325 CrossRef Medline
8. Cheng, V. C., Lau, S. K., Woo, P. C., and Yuen, K. Y. (2007) Severe acute respiratory syndrome coronavirus as an agent of emerging and reemerging infection. *Clin. Microbiol. Rev.* **20,** 660–694 CrossRef Medline
9. Zaki, A. M., van Boheemen, S., Bestebroer, T. M., Osterhaus, A. D., and Fouchier, R. A. (2012) Isolation of a novel coronavirus from a man with pneumonia in Saudi Arabia. *N. Engl. J. Med.* **367,** 1814–1820 CrossRef Medline

10. Hui, D. S., Azhar, E. I., Kim, Y. J., Memish, Z. A., Oh, M. D., and Zumla, A. (2018) Middle East respiratory syndrome coronavirus: risk factors and determinants of primary, household, and nosocomial transmission. *Lancet Infect. Dis.* CrossRef Medline
11. Li, F. (2015) Receptor recognition mechanisms of coronaviruses: a decade of structural studies. *J. Virol.* **89,** 1954–1964 CrossRef Medline
12. Yeager, C. L., Ashmun, R. A., Williams, R. K., Cardellichio, C. B., Shapiro, L. H., Look, A. T., and Holmes, K. V. (1992) Human aminopeptidase N is a receptor for human coronavirus 229E. *Nature* **357,** 420–422 CrossRef Medline
13. Raj, V. S., Mou, H., Smits, S. L., Dekkers, D. H., Müller, M. A., Dijkman, R., Muth, D., Demmers, J. A., Zaki, A., Fouchier, R. A., Thiel, V., Drosten, C., Rottier, P. J., Osterhaus, A. D., Bosch, B. J., and Haagmans, B. L. (2013) Dipeptidyl peptidase 4 is a functional receptor for the emerging human coronavirus-EMC. *Nature* **495,** 251–254 CrossRef Medline
14. Hofmann, H., Pyrc, K., van der Hoek, L., Geier, M., Berkhout, B., and Pöhlmann, S. (2005) Human coronavirus NL63 employs the severe acute respiratory syndrome coronavirus receptor for cellular entry. *Proc. Natl. Acad. Sci. U.S.A.* **102,** 7988–7993 CrossRef Medline
15. Li, W., Moore, M. J., Vasilieva, N., Sui, J., Wong, S. K., Berne, M. A., Somasundaran, M., Sullivan, J. L., Luzuriaga, K., Greenough, T. C., Choe, H., and Farzan, M. (2003) Angiotensin-converting enzyme 2 is a functional receptor for the SARS coronavirus. *Nature* **426,** 450–454 CrossRef Medline
16. Milewska, A., Zarebski, M., Nowak, P., Stozek, K., Potempa, J., and Pyrc, K. (2014) Human coronavirus NL63 utilizes heparan sulfate proteoglycans for attachment to target cells. *J. Virol.* **88,** 13221–13230 CrossRef Medline
17. Watanabe, R., Sawicki, S. G., and Taguchi, F. (2007) Heparan sulfate is a binding molecule but not a receptor for CEACAM1-independent infection of murine coronavirus. *Virology* **366,** 16–22 CrossRef Medline
18. Schultze, B., Krempl, C., Ballesteros, M. L., Shaw, L., Schauer, R., Enjuanes, L., and Herrler, G. (1996) Transmissible gastroenteritis coronavirus, but not the related porcine respiratory coronavirus, has a sialic acid (*N*-glycolylneuraminic acid) binding activity. *J. Virol.* **70,** 5634–5637 Medline
19. Schultze, B., Gross, H. J., Brossmer, R., and Herrler, G. (1991) The S protein of bovine coronavirus is a hemagglutinin recognizing 9-*O*-acetylated sialic acid as a receptor determinant. *J. Virol.* **65,** 6232–6237 Medline
20. Krempl, C., Schultze, B., and Herrler, G. (1995) Analysis of cellular receptors for human coronavirus OC43. *Adv. Exp. Med. Biol.* **380,** 371–374 CrossRef Medline
21. Huang, X., Dong, W., Milewska, A., Golda, A., Qi, Y., Zhu, Q. K., Marasco, W. A., Baric, R. S., Sims, A. C., Pyrc, K., Li, W., and Sui, J. (2015) Human coronavirus HKU1 spike protein uses *O*-acetylated sialic acid as an attachment receptor determinant and employs hemagglutinin-esterase protein as a receptor-destroying enzyme. *J. Virol.* **89,** 7202–7213 CrossRef Medline
22. Chan, C. M., Lau, S. K., Woo, P. C., Tse, H., Zheng, B. J., Chen, L., Huang, J. D., and Yuen, K. Y. (2009) Identification of major histocompatibility complex class I C molecule as an attachment factor that facilitates coronavirus HKU1 spike-mediated infection. *J. Virol.* **83,** 1026–1035 CrossRef Medline
23. Jeffers, S. A., Tusell, S. M., Gillim-Ross, L., Hemmila, E. M., Achenbach, J. E., Babcock, G. J., Thomas, W. D., Jr., Thackray, L. B., Young, M. D., Mason, R. J., Ambrosino, D. M., Wentworth, D. E., Demartini, J. C., and Holmes, K. V. (2004) CD209L (L-SIGN) is a receptor for severe acute respiratory syndrome coronavirus. *Proc. Natl. Acad. Sci. U.S.A.* **101,** 15748–15753 CrossRef Medline
24. Marzi, A., Gramberg, T., Simmons, G., Möller, P., Rennekamp, A. J., Krumbiegel, M., Geier, M., Eisemann, J., Turza, N., Saunier, B., Steinkasserer, A., Becker, S., Bates, P., Hofmann, H., and Pöhlmann, S. (2004) DC-SIGN and DC-SIGNR interact with the glycoprotein of Marburg virus and the S protein of severe acute respiratory syndrome coronavirus. *J. Virol.* **78,** 12090–12095 CrossRef Medline
25. Chan, C. M., Chu, H., Wang, Y., Wong, B. H., Zhao, X., Zhou, J., Yang, D., Leung, S. P., Chan, J. F., Yeung, M. L., Yan, J., Lu, G., Gao, G. F., and Yuen, K. Y. (2016) Carcinoembryonic antigen-related cell adhesion molecule 5 is an important surface attachment factor that facilitates entry of Middle East respiratory syndrome coronavirus. *J. Virol.* **90,** 9114–9127 CrossRef Medline
26. Earnest, J. T., Hantak, M. P., Li, K., McCray, P. B., Jr., Perlman, S., and Gallagher, T. (2017) The tetraspanin CD9 facilitates MERS-coronavirus entry by scaffolding host cell receptors and proteases. *PLoS Pathog.* **13,** e1006546 CrossRef Medline
27. Lee, A. S. (2014) Glucose-regulated proteins in cancer: molecular mechanisms and therapeutic potential. *Nat. Rev. Cancer* **14,** 263–276 CrossRef Medline
28. Ni, M., Zhang, Y., and Lee, A. S. (2011) Beyond the endoplasmic reticulum: atypical GRP78 in cell viability, signalling and therapeutic targeting. *Biochem. J.* **434,** 181–188 CrossRef Medline
29. Nain, M., Mukherjee, S., Karmakar, S. P., Paton, A. W., Paton, J. C., Abdin, M. Z., Basu, A., Kalia, M., and Vrati, S. (2017) GRP78 is an important host factor for Japanese encephalitis virus entry and replication in mammalian cells. *J. Virol.* **91,** e02274 Medline
30. Triantafilou, K., Fradelizi, D., Wilson, K., and Triantafilou, M. (2002) GRP78, a coreceptor for coxsackievirus A9, interacts with major histocompatibility complex class I molecules which mediate virus internalization. *J. Virol.* **76,** 633–643 CrossRef Medline
31. Honda, T., Horie, M., Daito, T., Ikuta, K., and Tomonaga, K. (2009) Molecular chaperone BiP interacts with Borna disease virus glycoprotein at the cell surface. *J. Virol.* **83,** 12622–12625 CrossRef Medline
32. Chan, J. F., Chan, K. H., Choi, G. K., To, K. K., Tse, H., Cai, J. P., Yeung, M. L., Cheng, V. C., Chen, H., Che, X. Y., Lau, S. K., Woo, P. C., and Yuen, K. Y. (2013) Differential cell line susceptibility to the emerging novel human betacoronavirus 2c EMC/2012: implications for disease pathogenesis and clinical manifestation. *J. Infect. Dis.* **207,** 1743–1752 CrossRef Medline
33. Lau, S. K., Lau, C. C., Chan, K. H., Li, C. P., Chen, H., Jin, D. Y., Chan, J. F., Woo, P. C., and Yuen, K. Y. (2013) Delayed induction of proinflammatory cytokines and suppression of innate antiviral response by the novel Middle East respiratory syndrome coronavirus: implications for pathogenesis and treatment. *J. Gen. Virol.* **94,** 2679–2690 CrossRef Medline
34. Zhou, J., Chu, H., Li, C., Wong, B. H., Cheng, Z. S., Poon, V. K., Sun, T., Lau, C. C., Wong, K. K., Chan, J. Y., Chan, J. F., To, K. K., Chan, K. H., Zheng, B. J., and Yuen, K. Y. (2014) Active replication of Middle East respiratory syndrome coronavirus and aberrant induction of inflammatory cytokines and chemokines in human macrophages: implications for pathogenesis. *J. Infect. Dis.* **209,** 1331–1342 CrossRef Medline
35. Chan, C. P., Siu, K. L., Chin, K. T., Yuen, K. Y., Zheng, B., and Jin, D. Y. (2006) Modulation of the unfolded protein response by the severe acute respiratory syndrome coronavirus spike protein. *J. Virol.* **80,** 9279–9287 CrossRef Medline
36. Versteeg, G. A., van de Nes, P. S., Bredenbeek, P. J., and Spaan, W. J. (2007) The coronavirus spike protein induces endoplasmic reticulum stress and upregulation of intracellular chemokine mRNA concentrations. *J. Virol.* **81,** 10981–10990 CrossRef Medline
37. DeDiego, M. L., Nieto-Torres, J. L., Jiménez-Guardeno, J. M., Regla-Nava, J. A., Alvarez, E., Oliveros, J. C., Zhao, J., Fett, C., Perlman, S., and Enjuanes, L. (2011) Severe acute respiratory syndrome coronavirus envelope protein regulates cell stress response and apoptosis. *PLoS Pathog.* **7,** e1002315 CrossRef Medline
38. Liao, Y., Fung, T. S., Huang, M., Fang, S. G., Zhong, Y., and Liu, D. X. (2013) Upregulation of CHOP/GADD153 during coronavirus infectious bronchitis virus infection modulates apoptosis by restricting activation of the extracellular signal-regulated kinase pathway. *J. Virol.* **87,** 8124–8134 CrossRef Medline
39. Fung, T. S., Liao, Y., and Liu, D. X. (2014) The endoplasmic reticulum stress sensor IRE1α protects cells from apoptosis induced by the coronavirus infectious bronchitis virus. *J. Virol.* **88,** 12752–12764 CrossRef Medline
40. Zhang, Y., Liu, R., Ni, M., Gill, P., and Lee, A. S. (2010) Cell surface relocalization of the endoplasmic reticulum chaperone and unfolded protein response regulator GRP78/BiP. *J. Biol. Chem.* **285,** 15065–15075 CrossRef Medline
41. Tsai, Y. L., Zhang, Y., Tseng, C. C., Stanciauskas, R., Pinaud, F., and Lee, A. S. (2015) Characterization and mechanism of stress-induced translo-

cation of 78-kilodalton glucose-regulated protein (GRP78) to the cell surface. *J. Biol. Chem.* **290,** 8049–8064 CrossRef Medline
42. Arap, M. A., Lahdenranta, J., Mintz, P. J., Hajitou, A., Sarkis, A. S., Arap, W., and Pasqualini, R. (2004) Cell surface expression of the stress response chaperone GRP78 enables tumor targeting by circulating ligands. *Cancer Cell* **6,** 275–284 CrossRef Medline
43. Gonzalez-Gronow, M., Selim, M. A., Papalas, J., and Pizzo, S. V. (2009) GRP78: a multifunctional receptor on the cell surface. *Antioxid. Redox Signal.* **11,** 2299–2306 CrossRef Medline
44. Woo, P. C., Wang, M., Lau, S. K., Xu, H., Poon, R. W., Guo, R., Wong, B. H., Gao, K., Tsoi, H. W., Huang, Y., Li, K. S., Lam, C. S., Chan, K. H., Zheng, B. J., and Yuen, K. Y. (2007) Comparative analysis of twelve genomes of three novel group 2c and group 2d coronaviruses reveals unique group and subgroup features. *J. Virol.* **81,** 1574–1585 CrossRef Medline
45. Huang, C., Qi, J., Lu, G., Wang, Q., Yuan, Y., Wu, Y., Zhang, Y., Yan, J., and Gao, G. F. (2016) Putative receptor binding domain of bat-derived coronavirus HKU9 spike protein: evolution of betacoronavirus receptor binding Motifs. *Biochemistry* **55,** 5977–5988 CrossRef Medline
46. Li, W., Hulswit, R. J. G., Widjaja, I., Raj, V. S., McBride, R., Peng, W., Widagdo, W., Tortorici, M. A., van Dieren, B., Lang, Y., van Lent, J. W. M., Paulson, J. C., de Haan, C. A. M., de Groot, R. J., van Kuppeveld, F. J. M., *et al.* (2017) Identification of sialic acid-binding function for the Middle East respiratory syndrome coronavirus spike glycoprotein. *Proc. Natl. Acad. Sci. U.S.A.* **114,** E8508–E8517 CrossRef Medline
47. Jindadamrongwech, S., Thepparit, C., and Smith, D. R. (2004) Identification of GRP 78 (BiP) as a liver cell expressed receptor element for dengue virus serotype 2. *Arch. Virol.* **149,** 915–927 CrossRef Medline
48. Tao, Y., Tang, K., Shi, M., Conrardy, C., Li, K. S., Lau, S. K., Anderson, L. J., and Tong, S. (2012) Genomic characterization of seven distinct bat coronaviruses in Kenya. *Virus Res.* **167,** 67–73 CrossRef Medline
49. Lau, S. K., Poon, R. W., Wong, B. H., Wang, M., Huang, Y., Xu, H., Guo, R., Li, K. S., Gao, K., Chan, K. H., Zheng, B. J., Woo, P. C., and Yuen, K. Y. (2010) Coexistence of different genotypes in the same bat and serological characterization of Rousettus bat coronavirus HKU9 belonging to a novel betacoronavirus subgroup. *J. Virol.* **84,** 11385–11394 CrossRef Medline
50. Ge, X., Li, Y., Yang, X., Zhang, H., Zhou, P., Zhang, Y., and Shi, Z. (2012) Metagenomic analysis of viruses from bat fecal samples reveals many novel viruses in insectivorous bats in China. *J. Virol.* **86,** 4620–4630 CrossRef Medline
51. Tong, S., Conrardy, C., Ruone, S., Kuzmin, I. V., Guo, X., Tao, Y., Niezgoda, M., Haynes, L., Agwanda, B., Breiman, R. F., Anderson, L. J., and Rupprecht, C. E. (2009) Detection of novel SARS-like and other coronaviruses in bats from Kenya. *Emerg. Infect. Dis.* **15,** 482–485 CrossRef Medline
52. Tao, Y., Shi, M., Chommanard, C., Queen, K., Zhang, J., Markotter, W., Kuzmin, I. V., Holmes, E. C., and Tong, S. (2017) Surveillance of bat coronaviruses in Kenya identifies relatives of human coronaviruses NL63 and 229E and their recombination history. *J. Virol.* **91**
53. Corman, V. M., Eckerle, I., Memish, Z. A., Liljander, A. M., Dijkman, R., Jonsdottir, H., Juma Ngeiywa, K. J., Kamau, E., Younan, M., Al Masri, M., Assiri, A., Gluecks, I., Musa, B. E., Meyer, B., Müller, M. A., *et al.* (2016) Link of a ubiquitous human coronavirus to dromedary camels. *Proc. Natl. Acad. Sci. U.S.A.* **113,** 9864–9869 CrossRef Medline
54. Graham, R. L., and Baric, R. S. (2010) Recombination, reservoirs, and the modular spike: mechanisms of coronavirus cross-species transmission. *J. Virol.* **84,** 3134–3146 CrossRef Medline
55. Guan, Y., Zheng, B. J., He, Y. Q., Liu, X. L., Zhuang, Z. X., Cheung, C. L., Luo, S. W., Li, P. H., Zhang, L. J., Guan, Y. J., Butt, K. M., Wong, K. L., Chan, K. W., Lim, W., Shortridge, K. F., *et al.* (2003) Isolation and characterization of viruses related to the SARS coronavirus from animals in southern China. *Science* **302,** 276–278 CrossRef Medline
56. Lau, S. K., Woo, P. C., Li, K. S., Huang, Y., Tsoi, H. W., Wong, B. H., Wong, S. S., Leung, S. Y., Chan, K. H., and Yuen, K. Y. (2005) Severe acute respiratory syndrome coronavirus-like virus in Chinese horseshoe bats. *Proc. Natl. Acad. Sci. U.S.A.* **102,** 14040–14045 CrossRef Medline
57. Reusken, C. B., Haagmans, B. L., Müller, M. A., Gutierrez, C., Godeke, G. J., Meyer, B., Muth, D., Raj, V. S., Smits-De Vries, L., Corman, V. M., Drexler, J. F., Smits, S. L., El Tahir, Y. E., De Sousa, R., van Beek, J., *et al.* (2013) Middle East respiratory syndrome coronavirus neutralising serum antibodies in dromedary camels: a comparative serological study. *Lancet Infect. Dis.* **13,** 859–866 CrossRef Medline
58. Haagmans, B. L., Al Dhahiry, S. H., Reusken, C. B., Raj, V. S., Galiano, M., Myers, R., Godeke, G. J., Jonges, M., Farag, E., Diab, A., Ghobashy, H., Alhajri, F., Al-Thani, M., Al-Marri, S. A., Al Romaihi, H. E., *et al.* (2014) Middle East respiratory syndrome coronavirus in dromedary camels: an outbreak investigation. *Lancet Infect. Dis.* **14,** 140–145 CrossRef Medline
59. Chu, H., Wang, J. J., Qi, M., Yoon, J. J., Wen, X., Chen, X., Ding, L., and Spearman, P. (2012) The intracellular virus-containing compartments in primary human macrophages are largely inaccessible to antibodies and small molecules. *PLoS ONE* **7,** e35297 CrossRef Medline
60. Chu, H., Wang, J. J., Qi, M., Yoon, J. J., Chen, X., Wen, X., Hammonds, J., Ding, L., and Spearman, P. (2012) Tetherin/BST-2 is essential for the formation of the intracellular virus-containing compartment in HIV-infected macrophages. *Cell Host Microbe* **12,** 360–372 CrossRef Medline
61. Chu, H., Zhou, J., Wong, B. H., Li, C., Chan, J. F., Cheng, Z. S., Yang, D., Wang, D., Lee, A. C., Li, C., Yeung, M. L., Cai, J. P., Chan, I. H., Ho, W. K., To, K. K., *et al.* (2016) Middle East respiratory syndrome coronavirus efficiently infects human primary T lymphocytes and activates the extrinsic and intrinsic apoptosis pathways. *J. Infect. Dis.* **213,** 904–914
62. Chu, H., Zhou, J., Wong, B. H., Li, C., Cheng, Z. S., Lin, X., Poon, V. K., Sun, T., Lau, C. C., Chan, J. F., To, K. K., Chan, K. H., Lu, L., Zheng, B. J., and Yuen, K. Y. (2014) Productive replication of Middle East respiratory syndrome coronavirus in monocyte-derived dendritic cells modulates innate immune response. *Virology* **454–455**, 197–205
63. Chen, Z., Zhang, L., Qin, C., Ba, L., Yi, C. E., Zhang, F., Wei, Q., He, T., Yu, W., Yu, J., Gao, H., Tu, X., Gettie, A., Farzan, M., Yuen, K. Y., and Ho, D. D. (2005) Recombinant modified vaccinia virus Ankara expressing the spike glycoprotein of severe acute respiratory syndrome coronavirus induces protective neutralizing antibodies primarily targeting the receptor binding region. *J. Virol.* **79,** 2678–2688 CrossRef Medline
64. Chan, C. M., Chu, H., Zhang, A. J., Leung, L. H., Sze, K. H., Kao, R. Y., Chik, K. K., To, K. K., Chan, J. F., Chen, H., Jin, D. Y., Liu, L., and Yuen, K. Y. (2016) Hemagglutinin of influenza A virus binds specifically to cell surface nucleolin and plays a role in virus internalization. *Virology* **494,** 78–88 CrossRef Medline
65. Nal, B., Chan, C., Kien, F., Siu, L., Tse, J., Chu, K., Kam, J., Staropoli, I., Crescenzo-Chaigne, B., Escriou, N., van der Werf, S., Yuen, K. Y., and Altmeyer, R. (2005) Differential maturation and subcellular localization of severe acute respiratory syndrome coronavirus surface proteins S, M, and E. *J. Gen. Virol.* **86,** 1423–1434 CrossRef Medline